Available online at www.sciencedirect.com
ScienceDirect
Journal of Theoretical Biology 251 (2008) 35–59
Journal of Theoretical Biology
www.elsevier.com/locate/yjtbi

Allometric scaling laws for water uptake by plant roots

Mario Biondini*

School of Natural Resource Sciences, North Dakota State University, Fargo, ND 58105, USA

Received 18 January 2007; received in revised form 14 November 2007; accepted 14 November 2007
Available online 22 November 2007

Abstract

This paper develops scaling laws for plant roots of any arbitrary volume and branching configuration that maximize water uptake. Water uptake can occur along any part of the root network, and thus there is no branch-to-branch fluid conservation. Maximizing water uptake, therefore, involves balancing two flows that are inversely related: axial and radial conductivity. The scaling laws are tested against the root data of 1759 plants from 77 herbaceous species, and compared with those from the WBE model. I further discuss whether the scaling laws are invariant to soil water distribution. A summary of some of the results follows. (1) The optimal radius for a single root (no branches) scales with volume as $r \approx volume^{\frac{2}{8+a}}$ $(0<a\leqslant 1)$. (2) The basic allometric scaling for root radius branches $(r_{i+1} = \beta * r_i)$ is of the form $\beta = f(N)^{\frac{2*\varepsilon(N)}{8+a}}$, where $f(N) = A(N)/(n_b * (1 + A(N)))$, n_b is the number of branches, and $A(N)$ and $\varepsilon(N)$ are functions of the number of root diameter classes (not constants as in the WBE model). (3) For large N, β converges to the β from the WBE model. For small N, the β's for the two models diverge, but are highly correlated. (4) The fractal assumption of volume filling of the WBE model are also met in the root model even though they are not explicitly incorporated into it. (5) The WBE model for rigid tubes is an asymptotic solution for large root systems (large N and biomass). (6) The optimal scaling solutions for the root network appears to be independent of soil water distribution or water demand. The data set used for testing is included in the electronic supplementary archive of the journal.

Keywords: Constructal theory; Root scaling; Root allometry; Scaling laws; Water uptake

1. Introduction

Biological diversity is in part a matter of size, and to achieve that diversity organisms must adjust their structure and function to the physical and biological constraints that size imposes (Brown et al., 2000). This simple proposition coupled with a wealth of measurements and observations has led to a much closer examination of the scaling relationships (also known as allometric or power laws) between the size of organisms and many of their functional and structural characteristics, like metabolic rates, the design of the respiratory and circulatory networks, etc. Brown et al. (2000) provided an extensive historical perspective on these efforts. The authors concluded that while the evidence for strong scaling laws is extensive and covers a large array of organisms, the published relationships are empirically derived and lack a model of sufficient power and generality to explain them. West et al. (1997) provided such a model. The hypothesis behind what became known as the WBE model was that: (a) biological rates are limited by the rate at which energy, materials, and waste can be distributed or removed from the areas that require or produce them; (b) the process requires a space filling fractal network that branches hierarchically to cover all parts of a three-dimensional body; and (c) the network has to minimize the time and energy required to distribute resources or collect waste. The result from designing such a network was that many anatomical and physiological features should scale as multiples of $\frac{1}{4}$, just as the empirical evidence indicated (West et al., 1997).

It is important to note, however, that the problem of designing an optimal network to supply or collect fluids was first investigated by Bejan (1997) using a methodology known as constructal theory. The main principle of constructal theory is that any distribution network is

*Tel.: +1 701 231 8208; fax: +1 701 231 7590.
E-mail address: Mario.Biondini@ndsu.edu

0022-5193/$ - see front matter © 2007 Elsevier Ltd. All rights reserved.
doi:10.1016/j.jtbi.2007.11.018

destined to remain imperfect (Bejan, 2000). Optimizing a fluid network, thus, is equivalent to optimizing the distribution of the imperfection which generates the geometry or shape of the system. For example, in point-area and point-volume flows, constructal theory predicts tree architectures which display two flow regimes: one highly resistive (transversal flow), and a less resistive one (longitudinal flow), that can be applied at any scale: from macroscopic to microscopic systems (Bejan, 2000). As I explain later, this dual flow regime is precisely what characterizes water flow in roots.

The initial WBE model, dealt mostly with the circulatory and respiratory systems (West et al., 1997), but it was later expanded to include vascular plants, mostly the above ground component of the xylem or phloem system of trees (West et al., 1999). Bejan's (2000) results are consistent with both Murray's laws (Sherman, 1981) regarding the optimal scaling of the radius for a network of rigid tubes ($\approx \frac{1}{3}$), and the WBE $\frac{1}{4}$ laws for the sum of the network cross section area.

There has been a substantial amount of debate about the WBE model regarding both the derived $\frac{1}{4}$ law and the fractal properties of the network (Brown et al., 1998; Dawson, 1998; Kurz and Sandau, 1998; Dodds et al., 2001; Kozlowski and Konarzewski, 2004; Brown et al., 2005). The WBE model, however, is still the most plausible explanation for many of the $\frac{1}{4}$ scaling patterns found in nature.

The WBE model deals mostly with what I refer to as "*closed networks*". In these networks the exchange of materials takes place almost entirely at the tip of the network (for example the micro-circulatory part of the circulatory system), while the rest of the network is mostly impermeable and acts only as a conduit for the fluids. Fluids, thus, are conserved as they flow through the network: $q_0 = q_k * N_k$, where q_k and N_k are the volume flow rates and the total number of branches at level k of the network (West et al., 1997). The fractal structure of the network is volume preserving from one branching generation to the other, thus fixing the scaling of the length component (West et al., 1997): $4/3 * \pi * (l_k/2)^3 * N_k \approx 4/3 * \pi * (l_{k+1}/2)^3 * N_{k+1}$ (l_k is the length of branches at level k). With the length scaling fixed, optimizing the network for fluid transport is tantamount to finding the scaling for the radius (r_k) that minimizes resistance to flow across the entire network, subjected to cost and volume constraints (Sherman, 1981; West et al., 1997).

A plant root system, conversely, can be called an "*open network*" since water uptake takes place (at different rates) along the entire network. Optimizing a network of this type involves balancing two flows that are inversely related. The first one involves minimizing flow resistance through the network, which is inversely related to the fourth power of the radius (Sharp, 1988). The second one involves maximizing radial conductivity (the flow of water into the root) which is inversely related to root radius (Roose and Fowler, 2004).

This paper investigates the scaling laws for a specific biological open network: the roots of herbaceous plants. The objectives are: (1) find the optimal scaling solution for the radius of a plant root system that maximizes water uptake for any arbitrary volume and branching configuration; (2) test the solution against an extensive data set of the actual root architecture of 77 herbaceous species; (3) compare the scaling results with those from the WBE model; and (4) discuss whether the optimal scaling solution depends on soil water distribution. The entire data set of the root architecture, and above- and belowground biomass for the 1759 plants from 77 species used for theory testing is included in the electronic supplementary archive of the journal.

I want to emphasize that for reasons of mathematical tractability, I used a highly simplified version of a root system, that nevertheless should broadly capture the flow dynamics of the network. I do not dwell on the details of the biology of root water or nutrient uptake, the structures and mechanisms associated with it, the complex interconnection of xylem vessels within and between root branches, or the problems of drought induced cavitations, all of which have been extensively discussed, among others, by Esau (1965), Steudle and Peterson (1998), Shane et al. (2000), Steudle (2000a,b, 2001), Hacke and Sperry (2001), Sperry et al. (2003), and Zwieniecki et al. (2003).

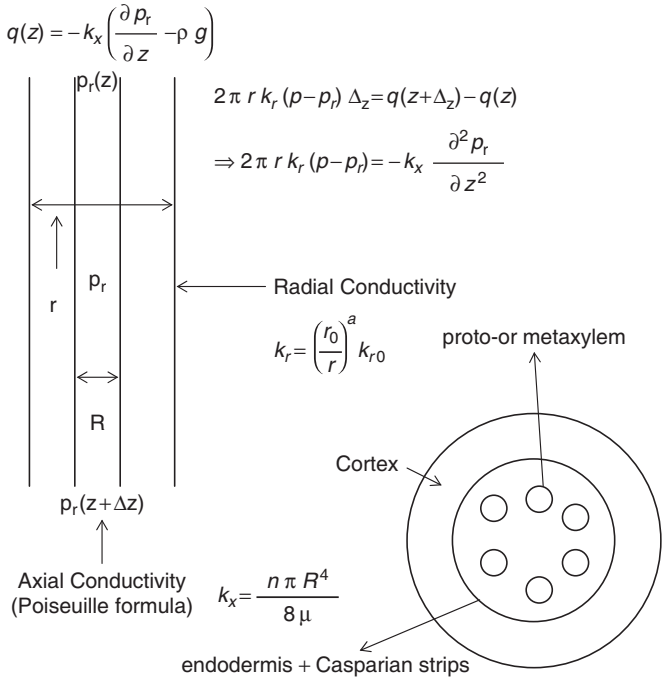

Fig. 1. Representation of a single root with the equations for the major water flows. The insert in the bottom right is a simplified schematic representation of the cross section of the root of a grass. $q(z)$ is water flow, $p_r(z)$ and p are the xylem and soil water pressures, k_x and k_r are the axial and radial conductivity, R and r are the xylem and root radiuses. For discussion of the equations and units see the text.

2. A theory of optimal root scaling for water uptake

I will use the following approach to find a scaling solution for the root radius that maximizes water uptake: (1) find an optimal solution for the case of a single root (no branching); (2) extend the solution for the main root with n_b first level branches (simple branching system); and (3) use the previous solution as the basic building block to construct a full root system with Bejan's constructal methodology for fluid trees (Bejan, 2000).

2.1. Single root case

The problem to be solved is as follows: *given a fixed root volume and uniform soil water pressure*, *determine what root radius maximizes water uptake* (Fig. 1). The first step in the process is to generate an equation for water flow within a single root. For that purpose I follow the approach of Roose (2000) and Roose and Fowler (2004). Water flow across a $z - z + \mathrm{d}z$ section of a root is equal to:

$$q(z) = -k_x * \left(\frac{\partial p_r}{\partial z} - \rho * g\right), \tag{1}$$

where $q(z)$ is the flow of water ($\mathrm{m^3\,s^{-1}}$) at any point z in the root ($z = 0$ at the top of the root), k_x is the axial conductivity ($\mathrm{m^4\,s^{-1}\,MPa^{-1}}$), pr is the water pressure (MPa) within xylem vessels, ρ is the density of water ($1\,\mathrm{Mg\,m^{-3}}$), and g is gravity ($9.8\,\mathrm{m\,s^{-2}}$). For a rigid tube, k_x can be estimated using Poiseuille's law for laminar flow (Sharp, 1988):

$$k_x = \frac{n * \pi * R^4}{8 * \mu}, \tag{2}$$

where n is the number of xylem vessels within a root segment, R (m) is the average radius of a xylem vessel, and μ (MPa s) is

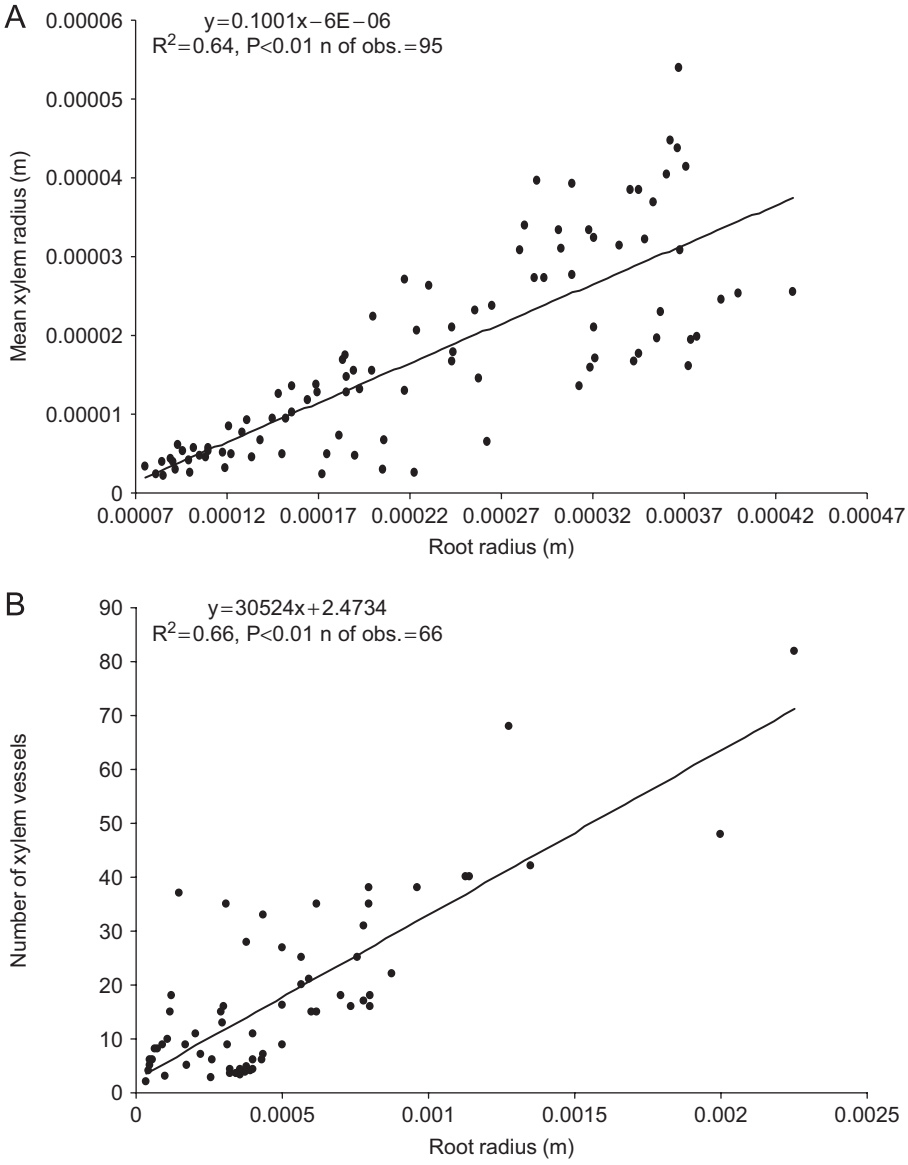

Fig. 2. Relationship between root radius and: (A) mean xylem tube radius; (B) mean number of xylem vessels. The regressions are from data for the 18 species listed in Table 1.

the kinetic viscosity of water (≈ 1.01 MPa s). If we take a Δ_z length of root and assume that there is a balance between the flow of water out of the root along the xylem and the flow of water into the root, then (Roose, 2000):

$$2\pi * r * k_r * (p - p_r) * \Delta_z = q(z + \Delta_z) - q(z)$$

$$\Rightarrow 2 * \pi * r * k_r * (p - p_r) = -k_x * \frac{\partial^2 p_r}{\partial z^2}, \quad (3)$$

where r is the root radius (m), and k_r is the root radial conductivity (m s^{-1} MPa^{-1}). Solving Eq. (3) for p_r results in the general solution:

$$p_r(z) = C_1 * e^{\frac{\kappa z}{l}} + C_2 * e^{-\frac{\kappa z}{l}} + p$$

and

$$\kappa = \sqrt{\frac{2 * \pi * r * k_r}{k_x}} * l, \quad (4)$$

where l (m) is the length of the root, p (MPa) is the soil water pressure, and C_1 and C_2 are constants that depend on the boundary conditions.

For the boundary conditions $p_r(0) = p_0$, and $\frac{\partial p_r}{\partial z}|_{z=l} = 0$, the solution for p_r and $\frac{\partial p_r}{\partial z}$ are

$$p_r(z) = \frac{p_0 - p}{1 + e^{2*\kappa}} * (e^{\frac{\kappa}{l}*z} + e^{\kappa*(2-\frac{z}{l})}) + p, \quad (5)$$

$$\frac{\partial pr}{\partial z} = \frac{\kappa}{l} * \frac{p_0 - p}{1 + e^{2*\kappa}} * (e^{\frac{\kappa}{l}*z} - e^{\kappa*(2-\frac{z}{l})}). \quad (6)$$

As a note, Eq. (5) is the same as Eq. (7) in Landsberg and Fowkes (1978) with two changes: (1) in their solution $z = l$ is the top of the root (soil surface); and (2) α^2 in their Eq. (6) is equal to κ^2/l in my notation. I followed Roose (2000) and use a coordinate system with $z = 0$ at the surface because it is a more natural one that allows for the simultaneous modeling of multiple roots with different lengths. One has to bear in mind that with this coordinate system water flow is negative (Eq. (1)) since $\frac{\partial p_r}{\partial z} \geqslant 0$ for all z.

By combining Eqs. (2) and (6) we can write Eq. (1) as

$$q(z) = -\frac{n * \pi * R^4}{8 * \mu} * \left[\frac{\kappa}{l} * \frac{p_0 - p}{1 + e^{2*\kappa}}(e^{\frac{\kappa}{l}*z} - e^{\kappa*(2-\frac{z}{l})}) - \rho * g\right]. \quad (7)$$

For most plants, particularly herbs, the term $\rho * g$ can be ignored (Landsberg and Fowkes, 1978), which from now on I do.

Maximizing water flow in a single root is equivalent to finding an r that minimizes Eq. (7) (water flow is negative) at $z = 0$, with the constraint of a fixed root volume (vol). To do that we first need to find a function to relate r to R (average xylem radius), n (number of xylem vessels), and k_r (radial conductivity). There is a limited amount of quantitative data describing the xylem dimension of roots, in particular herbaceous plants. A compilation of available data, however, shows that across a wide range of species both R and n are linearly related to r (Fig. 2). Furthermore, when the data is partitioned by species the linear relationships are even stronger (Table 1). I thus scale both R and n linearly with r: $R \approx b_R * r$ and $n \approx b_n * r$. With regard to k_r, Roose (2000) showed that it can be modeled as an inverse function of r of the form:

$$k_r = k_{r0} * \left(\frac{r0}{r}\right)^a,$$

where k_{r0} is the measured radial conductivity for a root of radius $r0$, and a is a scaling factor ($0 < a \leqslant 1$). While Roose (2000) uses an $a = 1$, I generalize the solution for an $0 < a \leqslant 1$ to account for the development of the Casparian strips and/or suberized exodermis (typical of older roots) that substantially reduces radial conductivity as a function of root radius (Esau, 1965; Peterson, 1988). One can now rewrite k_x and κ as

$$k_x = \frac{n * \pi * R^4}{8 * \mu} = \frac{b_n * r * \pi * (b_r * r)^4}{8 * \mu} = \frac{b * \pi * r^5}{8 * \mu}$$

where $b(\mathrm{m}^{-1}) = b_n * b_R^4$,

Table 1
Slope and R^2 for the linear relationship among root radius, average xylem radius, and number of xylem vessels across several species reported in the literature

Species	Average xylem radius (m) vs. root radius (m)		Number of xylem vessels vs. root radius (m)		References
	Slope	R^2 and P-value	Slope	R^2 and P-value	
Zea mays	0.030	0.80, $P<0.01$	33,213	0.96, $P<0.01$	Roose (2000)
Zea mays	0.023	0.87, $P<0.01$			Miller (1981)
Citrus aurantium, *Poncirus trifoliate*, and *Citrus paradisi*	0.017	0.87, $P<0.01$	1,04,155	0.66, $P<0.01$	Huang and Eissenstat (2000)
Oxya sative (12 varieties)	0.067	0.68, $P<0.01$	15,397	0.64, $P<0.01$	Kondo et al. (2000)
Zea mays	0.033	0.88, $P<0.01$	61,417	0.94, $P<0.01$	Li and Shao (2003)
Prunus persica			32,333	0.87, $P<0.01$	Vercambre et al. (2002)
Zea mays	0.12	0.82, $P<0.01$			Varney et al. (1991)
Data from 12 species from the following genera (two from each): *Senna*, *Bossiae*, *Pultenae*, *Atriplex*, *Hakea*, *Dodonaea*			51,544	0.70, $P<0.01$	Nicotra et al. (2001)

$$l = \frac{vol}{\pi * r^2}$$

$$\Rightarrow \kappa = \sqrt{\frac{2 * \pi * r * k_r}{k_x}} * l = \frac{4 * vol * \sqrt{\frac{k_{r0} * r0^a * \mu}{b}}}{\pi * r^{\frac{8+a}{2}}}, \tag{8}$$

and water flow at the top of the root [$q(0)$] as

$$q(0) = -\frac{b * \left(e^{\frac{8 * vol * \sqrt{\frac{k_{r0} * r0^a * \mu}{b}}}{\pi * r^{\frac{8+a}{2}}}} - 1 \right) (p - p_0) * \pi * r^{\frac{6+a}{2}} * \sqrt{\frac{k_{r0} * r0^a * \mu}{b}}}{2 * \mu * \left(e^{\frac{8 * vol * \sqrt{\frac{k_{r0} * r0^a * \mu}{b}}}{\pi * r^{\frac{8+a}{2}}}} + 1 \right)}. \tag{9}$$

To minimize $q(0)$ we need to find the value of r that satisfies $\frac{\partial q(0)}{\partial r} = 0$ and $\frac{\partial^2 q(0)}{\partial r^2} > 0$. The first equation can be written as follows:

$$\frac{\partial q(0)}{\partial r} = \frac{(p - p_0) * \left(16 * (8 + a) * e^{X(r)} * k_{r0} * r0^a * vol * \mu + (a - 6) * b * \frac{\pi^2 * r^{8+a} * X(r)}{8 * vol} * [e^{2 * X(r)} - 1] \right)}{4 * r^{2+a} * (1 + e^{X(r)})^2 * \mu} = 0, \tag{10}$$

where

$$X(r) = \frac{8 * vol * \sqrt{\frac{k_{r0} * r0^a * \mu}{b}}}{\pi * r^{\frac{8+a}{2}}}.$$

Multiplying the left and right side of Eq. (10) by $\frac{4 * r^{2+a} * (1 + e^{X(r)})^2 * \mu}{(p - p_0) * (a - 6) * b * \frac{\pi^2 * r^{8+a} * X(r)}{8 * vol}}$ we get the following equation to solve for $X(r)$ (which depends only on parameter a):

$$e^{2X(r)} = 1 - \frac{2 * (8 + a)}{a - 6} * X(r) * e^{X(r)}. \tag{11}$$

Eq. (11) has numerical solutions for $X(r)$ when values of $0 < a < 6$. It can also be shown that the solution for Eq. (11) also satisfies $\frac{\partial^2 q(0)}{\partial r^2} > 0$.

The solution of Eq. (11) combined with the definition of $X(r)$ provide us with the value of r that minimize $q(0)$. The optimal r, thus, scales with volume (vol) as follows:

$$r = vol^{\frac{2}{8+a}} * \left(\frac{8 * \sqrt{\frac{k_{r0} * r0^a * \mu}{b}}}{\pi * C} \right)^{\frac{2}{8+a}}, \tag{12}$$

where C is the numerical solution for Eq. (11) for a given a: $X(r) = C$. For $a = 1$ for example $C = 1.9861$.

Since for each individual plant the parenthesis values in Eq. (12) are constant, then r should scale with root volume as $r \approx vol^{\alpha}$ where $0.25 < \alpha \leqslant 0.22$. It is interesting to note

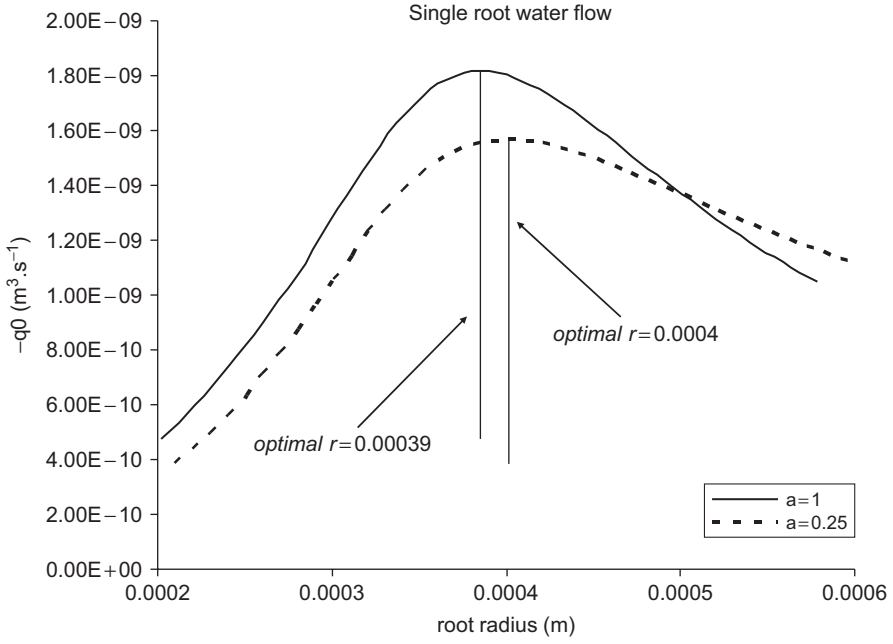

Fig. 3. Simulation of the rate of water uptake as a function of root radius (Eq. (9)) for a single root of the type shown in Fig. 1. The parameters used were: $vol = 1.57 * 10^{-7}\,m^3$, $\mu = 1.01 * 10^{-9}$ (MPa s); $k_{r0} = 2.5 * 10^{-7}$ (m s^{-1} MPa^{-1}); $r_0 = 5 * 10^{-4}$ (m); $C = 1.9861$; $p_0 = -12$ (MPa); $p = -3$ (MPa); $b = b_n * b_R^4 = 0.02728\,(m^{-1})$. For details see text.

that the optimal r is independent of both soil water pressure (p) and water demand (p_0). A numerical simulation of water uptake (Eq. (9)) is given in Fig. 3 for two values of a (the lower the a the larger the effects of suberized exodermis or Casparian strips). Both solutions have a minimum at the value defined by Eq. (12).

2.2. Simple branching system

The simple branching system to be optimized for water uptake (adapted from Roose, 2000) is shown in Fig. 4. Each branch has a root and xylem bundle structure similar to the one shown in Fig. 1. It is the basic unit that I will later use to construct water uptake for an entire root system.

In the previous section I modeled the flow of water within a single root by using a bundle of n xylem tubes, just as the WBE model does for vascular plants (West et al., 1999). In the WBE model, however, there is no bundle branching per se, but rather a split of the n_k tubes in a parent bundle into n bundles with n_{k+1} tubes, with the total number of tubes preserved: $n_k = n * n_{k+1}$. While this model applies to the xylem in stems and leaves, it does not represent well the xylem structure of roots where something closer to a true xylem bundle branching pattern exists. Lateral roots develop at some distance from the tip (where the apical meristem is located) and the base of the parent root (Esau, 1965), as schematically shown in Figs. 4 and 6. In both gymnosperms and angiosperms the lateral roots are initiated from the pericycle of the parent root and then break through the cortex (Esau, 1965). The xylem system of the lateral root is not a continuation of the parent root xylem, like in the WBE model (West et al., 1999), but rather develops independently from its own meristem tissue (Esau, 1965; Shane et al., 2000). There is therefore no implicit conservation of the total number of xylem tubes like in the WBE model. The xylem vessel bundles of the branch and main roots are then connected through an extensive vascular plexus of small diameter tracheary elements (also known as connecting xylem) (Esau, 1965; Shane et al., 2000). The root system, thus is best represented as true branching of xylem bundles with the number of xylem tubes and their average diameter dependent on the diameter of the parent and daughter roots. For a complete view of the structure and connection of parent root and daughter branches please consult Fig. 17.13 in Esau (1965), Figs. 1–7 in McCully and Mallett (1993), and Figs. 1–5 of Shane et al. (2000).

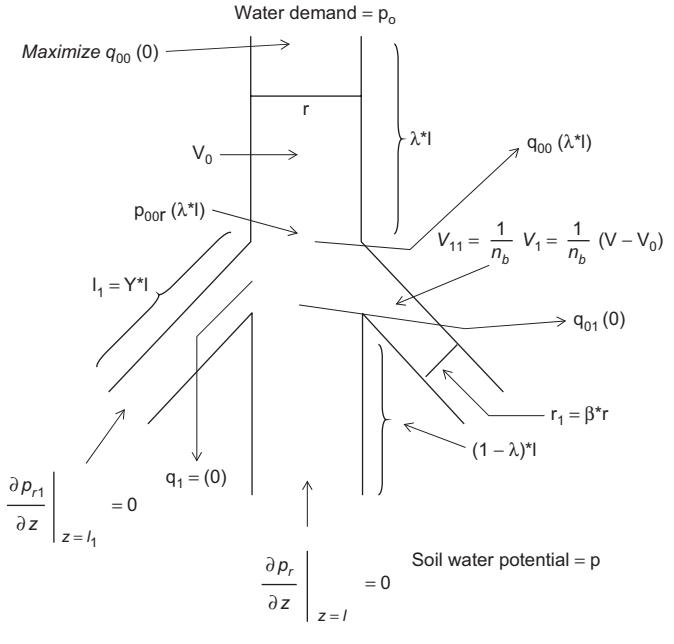

Fig. 4. Representation of a root simple branching system consisting of a parent root and 2 daughter branches (the parent and branches have a root and xylem bundle structure similar to the one shown in Fig. 1). V, V_0, and V_{11} (Eq. (15)) are the total, parent, and a daughter root volumes, n_b is the number of daughter branches (2 in this case), r, l, r_1, and l_1, are the parent and daughter root radius and lengths, p_{00r} and q_{00} are water pressure and flow rate in the parent root at or above the junction with the daughter roots, q_{01} is the water flow rate in the parent root at or below the junction with the daughter roots, q_1 is the water flow in the daughter branches, and γ, β, and λ are constants. For details see text.

Because of the complexity of the connections between the parent and daughter xylem bundles, I do not directly model each xylem vessel. Rather, what I model is the total flow of water entering the parent xylem bundle from the daughter xylem bundle and the concomitant changes in water flow and pressure at the junction. For purposes of mathematical tractability I do not include the potential effects of water pressure equalization that result from various degrees of connectivity between xylem vessels within a bundle (Esau, 1965). Also for mathematical simplicity I assume that all branching occurs at a fixed point in the root rather than at various parts along the root.

The total volume (V) of the branching system in Fig. 4 is partitioned into V_0 for the main stem and V_1 for the n_b branches (each branch thus has a volume of $1/n_b * V_1$). The radius of the main stem is r, while the radius of each branch is $r_1 = \beta * r$. The length of the main stem is l which is divided into $\lambda * l$ and $(1 - \lambda) * l$ $(0 < \lambda < 1)$ based on the point of insertion of the lateral branches. The length of each of the lateral branches is $l_1 = \gamma * l$. The reader should notice that I am using the same β and γ notation of the WBE model (West et al., 1997). The problem to be solved is as follows: *given a fixed root volume* $(V = V_0 + V_1)$, n_b *branches*, *uniform soil water pressure* (p), *and a fixed water pressure at the top of the main stem* (p_0), *find the values for* β *and* γ *that maximize water uptake* ($q[0]$).

The first step in solving this problem is to properly define V, V_0, and V_1 within the context of the entire root system. This is necessary because the volume relationships between main stem and branches in the simple branching system has to reflect the actual relationships for the entire root system. A model for the distribution of volume (biomass) within a root system has to fit a series of requirements based on the known anatomy and growth patterns of roots. Among them: (1) root growth occurs in the apical zone of each branch (Esau, 1965), consequently most of the root volume

and length, has to be located in the terminal branches (Johnson and Biondini, 2001; Levang-Brilz and Biondini, 2002); (2) plant growth rates follow logistic patterns (Biondini, 2001; Levang-Brilz and Biondini, 2002), consequently the rate of increase in root total volume should decline with the number of root nodes (diameter classes); (3) based on the scaling laws found for other branching networks, like the respiratory and cardiovascular one (West et al., 1997; Bejan, 2000), as well as empirical data on roots (Johnson and Biondini, 2001; Levang-Brilz and Biondini, 2002), the volume of the root branch of order zero should scale as a power function of the total number of diameter classes; finally (4) the model has to fit empirical data.

Based on requirements listed above I use the following model for root volume distribution as a function of diameter classes:

$$V_0(N) = v_0 * N^{\delta_0},$$

$$V(i) = V_0(N) * A(N)^i \quad \text{for } 0 \leqslant i \leqslant N,$$

$$V_i(N) = V_0(N) * A(N)^i * (1 - A(N)^{-1}) \quad \text{for } 1 \leqslant i \leqslant N,$$

$$A(N) = e^{\frac{\eta}{N^\rho}},$$

$$N_i \approx n_b^i, \quad 0 \leqslant i \leqslant N, \tag{13}$$

where N is the total number of root diameter classes (branch orders), N_i is the total number of root branches for root diameter class i ($0 \leqslant i \leqslant N$), $V_0(N)$ is the volume of root branches of order zero, $V(i)$ is the cumulative volume of the root system up to and including branches of diameter class i [total root volume $= V(N)$], $V_i(N)$ is the volume of only branches of diameter class i [$V_i(N) = V(i) - V(i-1)$], and v_0, δ_0, η and ρ are constants that need to be experimentally determined. As in the WBE model (West et al., 1997), I modeled N_i as a power function of n_b. $A(N)$ has the following characteristics: $A(N) \geqslant 1$ for all N, and $A(N) \to 1$ as $N \to \infty$. Finally, the model meets the requirement that the relative growth rate of volume decline with N:

$$\frac{1}{V(N)} * \frac{dV(N)}{dN} = \frac{\delta_0}{N} + \eta * \frac{1-\rho}{N^\rho} \to 0 \quad \text{as } N \to \infty. \tag{14}$$

The various elements of the root volume model were tested using data from 1759 plants, of 77 species, and at multiple stages of growth (see the Testing section). As shown in Table 2 the model showed a high level of accuracy in describing the empirical root volume data.

With Eq. (13), we can now define V, V_0, and V_1 in the simple branching system (Fig. 4). Any sector of the branching structure of a root produces a main stem and n_b branches with the following volumes:

$$V_0 = V_0(N) * (1 - A(N)^{-1}) * \left(\frac{A(N)}{n_b}\right)^i, \quad 1 \leqslant i \leqslant N,$$

$$V_1 = V_0(N) * (1 - A(N)^{-1}) * n_b * \left(\frac{A(N)}{n_b}\right)^{i+1} = A(N) * V_0, \quad 1 \leqslant i \leqslant N-1,$$

$$V = V_0 * (1 + A(N)), \tag{15}$$

where N, $V_0(N)$, and $A(N)$ are as defined in Eq. (13).

With the volumes defined, we can now find the solution for β and γ that maximize water uptake for a simple branching system. The complete derivation of the solution is shown in Appendix A. The pertinent equations are

$$\beta = \left(\frac{A(N)}{n_b * (1 + A(N))}\right)^{\frac{2}{8+a}},$$

$$\gamma = \frac{A(N)}{n_b} * \beta^{-2}. \tag{16}$$

As was the case for a single root, the optimal values for β and γ are also independent of p and p_0, as well as of r and λ.

Fig. 5 shows a numerical simulation of water flow for a simple branching system: $q(0)$ (Eq. (A.7)). The simulation shows that the optimal value of β that maximizes water uptake is as defined by Eq. (16): $\beta = (\frac{1.37}{2*2.37})^{\frac{2}{9}} = 0.7589$.

2.3. Complete root system

The network to be modeled is shown in Fig. 6. The network chosen is general enough to accommodate the two topological ends of the spectrum of root types described by Fitter (1987) and Taub and Goldberg (1996): maximally herringbone (a simple branching system with $N = 1$ and large n_b), and maximally dichotomous (large N and $n_b \approx 2$). Other intermediate forms (which I will not deal with here) can be easily created by making n_b a function of root order [$n_{bi} = f(i)$]. The proposed network is a generalization of the WBE model designed to accommodate: (a) water absorption along the entire network, as well as

Table 2
Relationships between the estimates (Eq. (13)) of total root volume [V(N)], and volume for roots of order 0 [V_0(N)], and the actual measurements of V(N), V_0(N), and root biomass (RB)

Relationship (Y vs. X)	Equation	R^2	P-value	Slope 95% CI
ln actual V (mm^3) vs. ln RB (g)	$Y = 7.8 + 1.07 * X$	0.78	0.0001	± 0.020
ln actual V (mm^3) vs. ln estimated V (mm^3)	$Y = -0.24 + 0.98 * X$	0.98	0.0001	± 0.010
ln actual V_0 (mm^3) vs. ln estimated V_0 (mm^3)	$Y = -0.64 + 0.84 * X$	0.95	0.0001	± 0.015

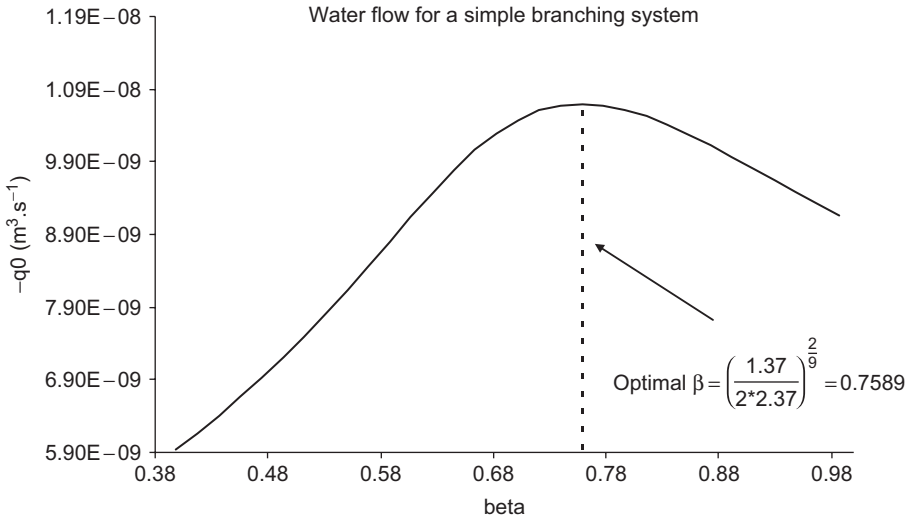

Fig. 5. Simulation of water uptake as a function of β (Eq. (A.7)) for a simple branching system of the type shown in Fig. 4. The parameters used were $V_0 = 9.2 * 10^{-7}\,\mathrm{m}^3$; $V_1 = 1.26 * 10^{-6}\,\mathrm{m}^3$; $A = 1.37$; $\lambda = 0.2$; $n_b = 2$; $a = 1$; $r = 6.9 * 10^{-4}\,\mathrm{m}$; $\mu = 1.01 * 10^{-9}$ (MPa s); $C = 1.9861$; $p = -3$ (MPa); $p_0 = -12$ (MPa); $k_{r0} = 2.5 * 10^{-7}\,(\mathrm{m\,s^{-1}\,MPa^{-1}})$; $r_0 = 5 * 10^{-4}\,(\mathrm{m})$; $b = b_n * b_R^4 = 0.02728\,(\mathrm{m^{-1}})$. For details see text.

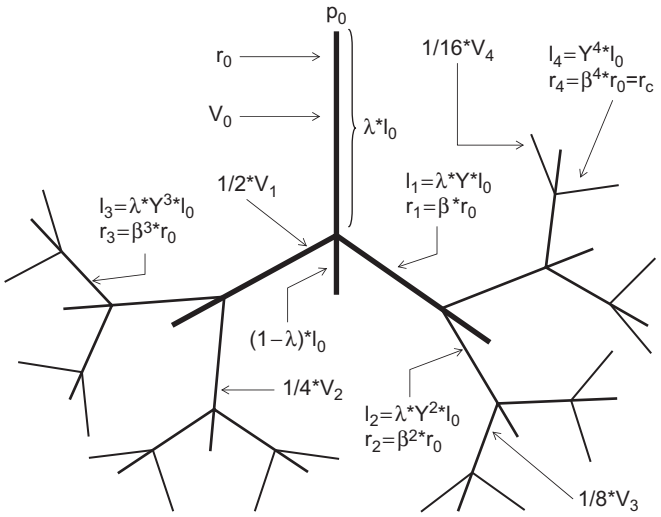

Fig. 6. Schematic representation of a root network with $N = 3$ and $n_b = 2$. Symbols as described in Fig. 4. See text for details.

flow through the network; and (b) the root anatomical aspects discussed in the previous section.

The network is built using Bejan (2000) constructal methodology for fluid trees by connecting together the basic units shown in Fig. 4 and described in detail in the previous section and Appendix A. The volume, and total number of root branches per root diameter class (V_i and N_i) are modeled as in Eq. (13). The scaling constraints for length and radius follow Eq. (16). In building a full root model, however, there are two extra details that need to be included: (1) the proper value for r_0 (the radius for branches of order 0); and (2) ensuring that as N increases the root radius for the terminal branches (r_N) does not decline toward zero.

As shown for the single root case (Eq. (12)), r_0 scales with root volume. The problem, however, is to determine the scaling factor for a full root system. At r_0 we have a transition between the open network of the roots and the closed network of the stems and leaves. If we were to consider r_0 exclusively as node 0 of the root system then it should scale as in Eq. (12). Conversely, if we consider it as node 0 of the stem and leaves closed system of rigid tubes, then according to West et al. (1997) it should scale as $\frac{1}{3}$ of the volume (or biomass) of the above-ground xylem. In the original WBE model the scaling for r_0 is $\frac{3}{8}$ because they use a $\frac{1}{2}$ scaling for r_i. For a system of rigid tubes, however, West et al. (1997) show that the proper scaling for r_i follows Murray's law of $\frac{1}{3}$, which results in a $\frac{1}{3}$ scaling for r_0. The scaling for r_0 has to be solved empirically (see the Testing section), thus I will use a generic scaling of α as a place holder: $r_0 \approx V(N)^{\alpha}$ (since in grasses and forbs above ground biomass is a linear function of below ground biomass [Johnson and Biondini, 2001; Levang-Brilz and Biondini, 2002]). Specifically r_0 is modeled as

$$r_0 = rconst * V(N)^{\alpha}. \tag{17}$$

For single roots (Eq. (12))

$$rconst = \left(\frac{8 * \sqrt{\dfrac{k_{r0} * r0^{a} * \mu}{b}}}{\pi * C} \right)^{\frac{2}{8+a}} \quad \text{and} \quad \alpha = 2/(8+a).$$

For the general case however *rconst* and α have to be fitted empirically (see Testing section).

To ensure that as N increases the root radius of terminal branches (r_N) does not decline toward zero, I used the same assumption of West et al. (1997), that the radius of the terminal branches (i.e. the smallest root radius) is constant

and independent of N (and thus volume): $r_N = \beta^N * r_0 = r_c$ for all N. To achieve that β (Eq. (16)) has to be scaled by a constant ε as follows:

$$(\beta^{\varepsilon(N)})^N * r_0 = \left(\overset{*}{\beta}\right)^N * r_0 = \left[\left(\frac{A(N)}{n_b * (1 + A(N))}\right)^{\frac{2*\varepsilon(N)}{8+a}}\right]^N * r_0 = r_c$$

$$\Rightarrow \varepsilon(N) = \frac{(8 + a) * \ln\left(\frac{r_c}{r_0}\right)}{2 * N * \ln\left(\frac{A(N)}{n_b * (1 + A(N))}\right)}. \quad (18)$$

It can be shown that $\overset{*}{\beta} < 1$ for all $N < \infty$. For the remainder of this section I will use β for $\overset{*}{\beta}$.

With these two adjustments, we can then calculate the length and radius for each branch order in the root system (Fig. 6) as

$$\gamma = \frac{A(N)}{n_b} * \beta^{-2}, \quad r_i = \beta^i * r_0,$$
$$l_0 = \frac{\lambda * V_0}{\pi * r_0^2}, \quad l_1 = \frac{(1-\lambda) * \lambda * V_0}{\pi * r_0^2},$$
$$l_{0,i} = \frac{\lambda * V_i}{\pi * n_b^i * r_i^2}, \quad l_{1,i} = \frac{(1-\lambda) * V_i}{\pi * n_b^i * r_i^2}, \quad 0 < i < N-1,$$
$$l_N = \frac{V_N}{\pi * n_b^N * r_N^2} \quad \text{where } r_N = r_c \text{ for all } N. \quad (19)$$

Appendix B provides a description of the numerical methodology needed to calculate water uptake for any network configuration of the type shown in Fig. 6. Figs. 7A–B show examples for the values of $\varepsilon(N)$, and α that maximize water uptake. In Fig. 7A $\varepsilon(N)$ is varied keeping $\alpha = \frac{2}{9}$. The optimal $\varepsilon(N)$ that maximizes water uptake is equal to the solution provided by Eq. (18) for the parameters used in the model: $\varepsilon(N) = 1$. In Fig. 7B, α is varied, while $\varepsilon(N)$ is kept at its theoretical value of $\varepsilon(N) = 1$. The optimal α that maximizes water uptake is equal to $\alpha = \frac{2}{9}$ which is the solution provided by Eq. (12). This was expected since the model deals exclusively with r_0

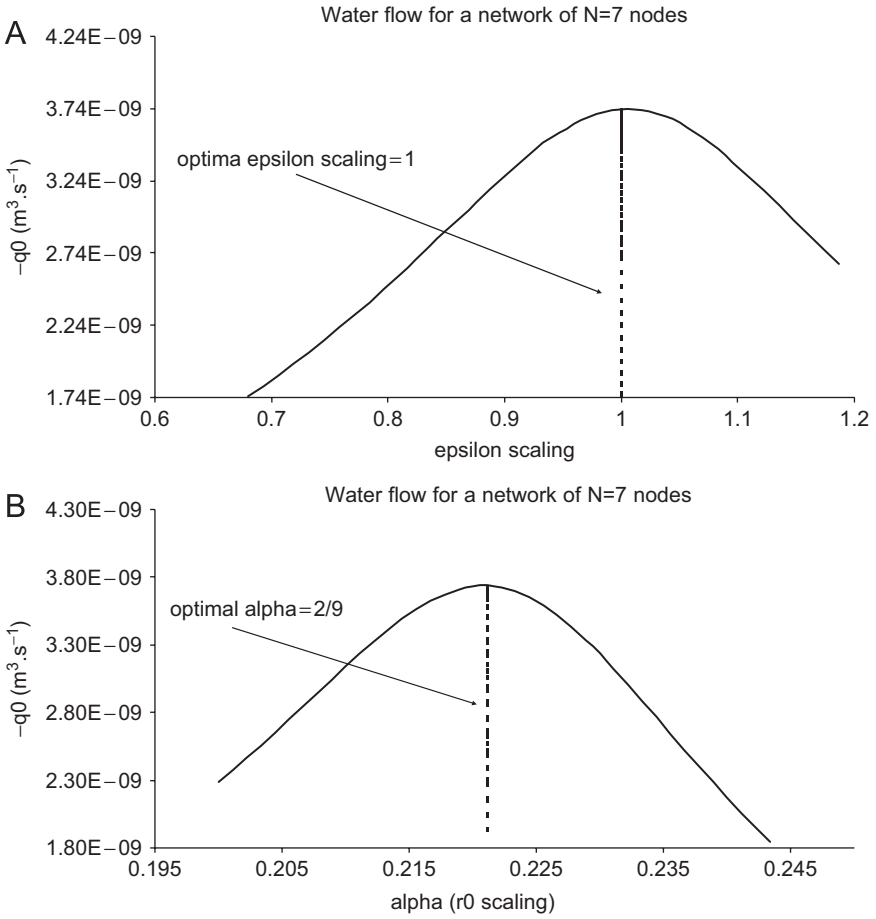

Fig. 7. Simulation of water uptake for a root network of $N = 7$ (Eq. (B.5)). The parameters used were $N = 7$; $n_b = 2$; $v_0 = 2.0 * 10^{-12}$ (m^3); $\delta_0 = 2.0828$; $\eta = 4.7407$; $\rho = 1.0037$; $a = 1$; $r_c = 3.95 * 10^{-5}$ plus the ones listed in Fig. 5. (A) Water uptake as a function of $\varepsilon(N)$ (Eq. (18)). (B) Water uptake as a function of α (Eq. (17)).

as node 0 of the root system. These runs, plus others not shown, confirm that the theoretical scaling parameters for α, β, and $\varepsilon(N)$ defined by Eqs. (12), (16)–(18) are the optimal for root networks of the type shown in Fig. 6.

3. Theory testing

To test some of the theoretical relationships developed in the previous section, I used data on the root architecture of 1759 plants from the 77 species shown in Table C.1. The root data provided information on: (1) number of root diameter classes (N); (2) the diameter of each diameter class ($2 * r_i$, $0 \leqslant i \leqslant N$); (3) number of root branches per diameter class (N_i); (4) the root length, surface area, and volume per each diameter class; and (5) total above-ground and root biomass. For details on the experimental design and methodologies used to generate the data see Appendix C.

3.1. Root volume and branching pattern

The first test was to compare root volume with root biomass across all 1759 plants. The purpose was to check the accuracy of the methods used to estimate volume (Appendix C), since root volume should be related to root biomass. The second test was to compare the actual root volume and branching data with the ones predicted by Eq. (13) across all plants. For each of the 1759 plants, I ran a regression between the ln actual $V(i)$ vs. i (where i is root diameter class, $0 \leqslant i \leqslant N$, and $V(i)$ the cumulative root volume up to and including node i). If Eq. (13) is correct, the fit should be high with the intercept $= \ln V_0(N)$, and the slope $= \ln A(N)$. For each plant, then, the expected $\ln V(N)$ is the value of the fitted equation at $i = N$. The third test was to regress for each plant $\ln N_i$ vs. i. If the branching pattern described in Eq. (13) is correct, then the fit should be high and the slope $= \ln n_b$.

Table 2 shows results for the regression between $V(N)$ and root biomass, and the expected and actual $V(N)$ and $V_0(N)$ relationships across all plants. In all cases the correlations are high. In the case of $V(N)$ the slopes of the regressions are close to one, while for $V_0(N)$ it is slightly lower than one indicating an overestimation of $V_0(N)$ by Eq. (13). Fig. 8 shows the relationship between the $\ln A(N)$ vs. N across all plants which fits well the exponential model of Eq. (13). Fig. 9A shows the summary of R^2 values for all the regressions of $\ln N_i$ vs. i, while Fig. 9B shows the relationship between the estimated n_b and N across all plants. Fig. 9A indicates a robust fit for the model $N_i \approx n_b^i$ across all plant sizes (the median $R^2 = 0.92$ and the first quartile $= 0.85$). Fig. 9B shows an interesting pattern: n_b declines as a power function of N reaching an asymptotic $n_b \approx 1.2$ for large N.

3.2. Radius and length scaling patterns

To test the basic theoretical root scaling relationship (Eqs. (16)–(19) and (B.7)–(B.9)) I proceeded in the following manner. To estimate the empirical values of β, I ran a regression between $\ln r_i$ vs. i for each of the 1759 plants. If Eq. (19) is correct, then the fit should be high, and the regression slope equal to the ln *actual* β. The theoretical β was calculated with Eq. (18) as

$$\beta = \left(\frac{A(N)}{n_b * (1 + A(N))}\right)^{\frac{2*\varepsilon(N)}{8+a}},$$

where a was arbitrarily set as $a = 1$ for all plants, and n_b and $A(N)$ are the empirical values for each plant estimated as shown in the previous section. $\varepsilon(N)$ was calculated with Eq. (18) using the measured values of r_0 and r_N ($r_c = r_N$) for the 1759 plants.

I calculated the actual scaling relationship between total length for root class i (Tl_i) with i and r_i by running regressions between $\ln Tl_i$ vs. i and $\ln Tl_i$ vs. $\ln r_i$ for each of the 1759 plants. The slope of the regression was the

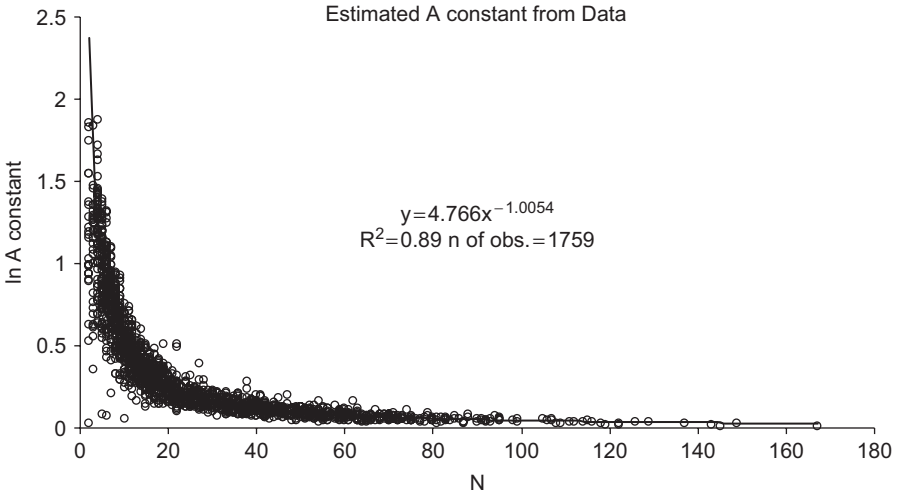

Fig. 8. Estimation of $A(N)$ from empirical data: 1759 plants from 77 species (see Appendix C and Table C.1).

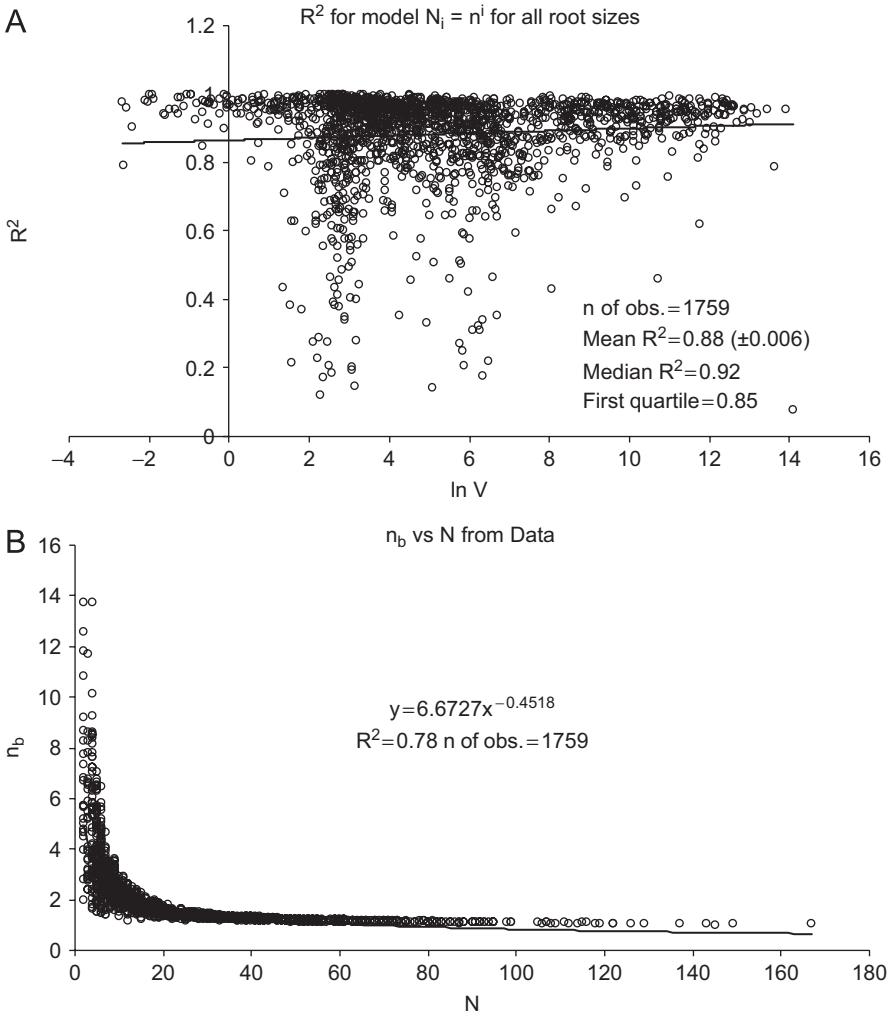

Fig. 9. (A) R^2 values from fitting $\ln N_i = i * \ln n_b$ (N_i is total number of root branches per root diameter i) as a function of the ln V of 1759 plants from 77 species (see Appendix C and Table C.1). (B) Empirical estimation of n_b as a function of N for the same data set. n_b is the exponential of the slope from fitting $\ln N_i = i$ (Eq. (13)).

empirical scaling value. The theoretical values are as shown in Eqs. (20)–(21) (for a proof see Eqs. (B.7)–(B.9))

$$\ln r_i(N) \approx \ln\left(n_b^{\frac{4*\varepsilon(N)}{8+a}} * A(N)^{\frac{8+a-4*\varepsilon(N)}{8+a}} * (1+A(N))^{\frac{4*\varepsilon(N)}{8+a}}\right) * i, \tag{20}$$

$$\ln Tl_i(N) \approx \frac{\ln\left(n_b^{\frac{4*\varepsilon(N)}{8+a}} * A(N)^{\frac{8+a-4*\varepsilon(N)}{8+a}} * (1+A(N))^{\frac{4*\varepsilon(N)}{8+a}}\right)}{\frac{2*\varepsilon(N)}{8+a} * \ln\left(\frac{A(N)}{n_b*(1+A(N))}\right)} * \ln r_i \tag{21}$$

with $a = 1$, and the values for n_b, $A(N)$, and $\varepsilon(N)$ calculated from the actual data as shown above.

Finally, to compare the theoretical scaling relationships of r_0 vs. the empirical one I conducted two analyses: (1) compare the empirical $\ln r_0$ with the expected one (the intercept of the regression $\ln r_i$ vs. i used to estimate β); and (2) estimate the scaling value α for Eq. (17) by regressing $\ln r_0$ vs. $\ln V(N)$. For these relationships I used only the 1517 plants for which I had a complete accounting of root volume (data from the soil coring experiments was excluded).

Figs. 10A–B show the results regarding β. There was a strong correlation between $\ln r_i$ vs. i across the entire root volume spectrum. The actual and theoretical values of β are highly correlated and statistically similar for large N. Figs. 11A–B show the values for the actual vs. theoretical slopes for the $\ln Tl_i$ vs. i, and $\ln Tl_i$ vs. $\ln r_i$ relationships. The actual and theoretical (Eq. (20)) slopes for $\ln Tl_i$ vs. i are statistically undistinguishable (Fig. 11A). The regression fit is less tight for the actual and theoretical slopes (Eq. (21)) of $\ln Tl_i$ vs. $\ln r_i$ (Fig. 11B), even though it is still statistically significant (Eq. (21) overestimated the actual slope).

Fig. 12A shows that the fitted r_0 and empirical r_0 are highly correlated something that was expected given the

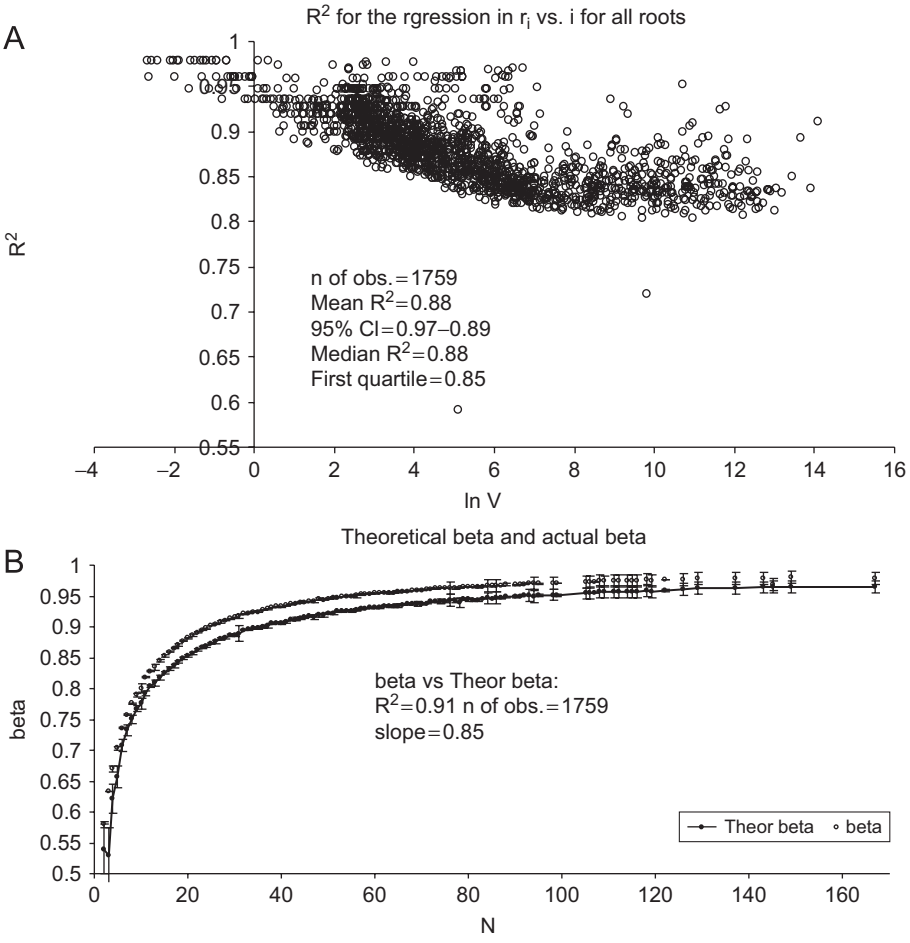

Fig. 10. (A) R^2 values from fitting $\ln r_i = i$ as a function of the ln V of 1759 plants from 77 species (see Appendix C and Table C.1). (B) Values for the theoretical β (Eq. (18)) and the empirical β (exponential of the slope from fitting $\ln r_i = i$) for the same data set. The vertical bars are the 95% CI.

excellent fit of the regression $\ln r_i$ vs. i (Fig 10a). Of further interest is the fact that both have a logarithmic relationship with N which is what Eq. (13) suggests: $V_0(N) = l_0 * \pi * r_0^2 = \upsilon_0 * N^{\delta 0}$, thus $\ln r_0 \approx \ln N$. Fig. 12B shows that $\ln r_0$ is in fact correlated with the $\ln V(N)$ (as predicted by Eq. (17)) with a scaling value of $\alpha = 0.3 \pm 0.023$ (for an interpretation of this result please see the Discussion).

3.3. Scaling of total length and root surface area

The theoretical relationships of root length (RL), and root surface area (RSA) with $V(N)$ are complex functions (Eqs. (B.10)–(B.11)). Simulations with a variety of α scaling values for r_0 (ranging from $\frac{2}{9}$ to $\frac{1}{3}$), show that the relationship can be approximated with a power function of $V(N)$ ($\ln RSA$ or $\ln RL \approx x * \ln V(N)$) with the scaling factor x ranging from 0.95 for low $V(N)$ to 0.75 for very large $V(N)$. The WBE model for rigid tubes (West et al., 1997) predicts a scaling for RSA and RL with mass (a proxy for volume) of 1. Table 3 shows the empirical results for the actual data (as before it includes only the 1517 plants for which I had a complete accounting of root biomass). The results fall within the simulation range and are always statistically lower than the scaling of 1 predicted by the WBE model.

4. Discussion

The power function used to describe the root volume distribution by root diameter class (Eq. (13)) fit the data with a high degree of accuracy across 1759 plants from 77 species (Table 2, Fig. 8). It is important to recognize that these equations were not derived from first principle so it is likely that other ones can be used for the same purpose. Alternative models, however, would have to meet at least the four requirements specified in the description of Eq. (13). It is important to note, also, that these equations can be used to model biomass distribution within a root system because of the high correlation between volume and biomass (Table 2).

The theoretical β (Eq. (18)) is statistically similar to the empirically derived one for large N (Fig. 10B), and significantly correlated for all $N(R^2 = 0.91,\ P < 0.00001)$. I also compared the empirical β with the one derived from the rigid tubes version of the WBE model (West et al., 1997) using the estimated n_b values: $WBE\,\beta = (1/n_b)^{1/3}$.

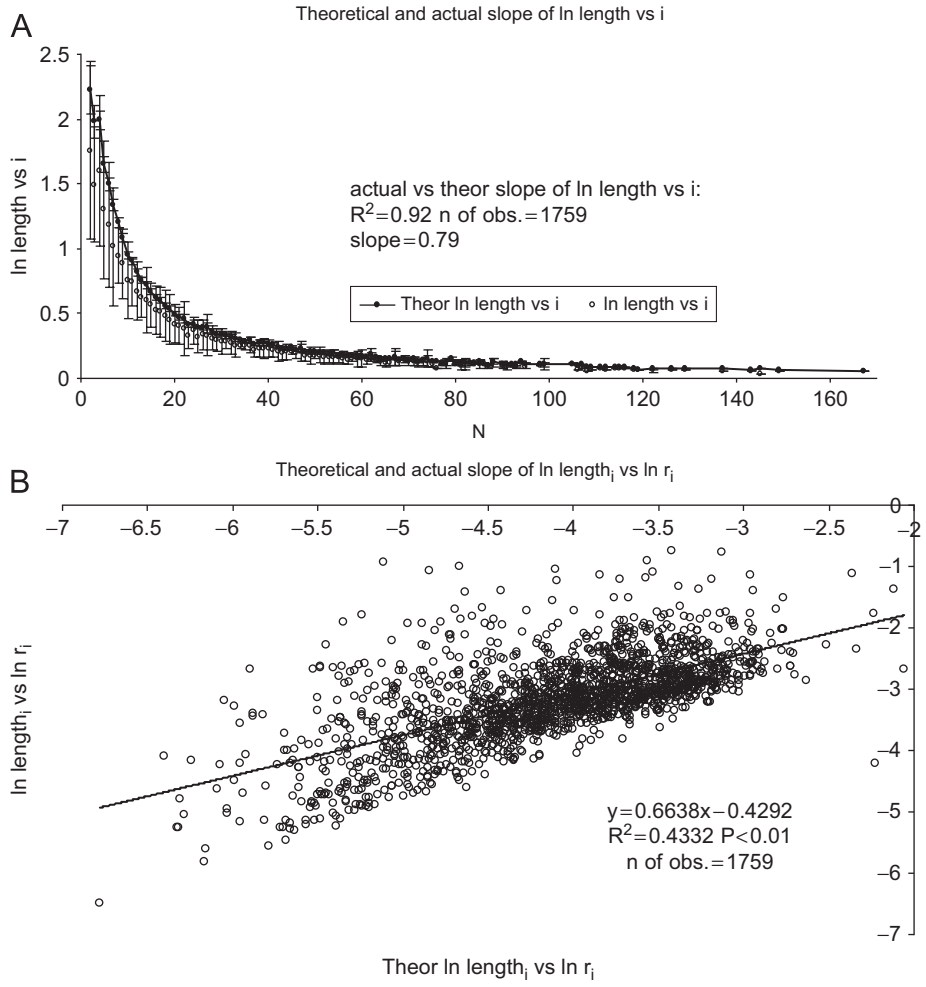

Fig. 11. (A) Theoretical (Eq. (20)), and empirical slopes for the relationship between ln Tl_i vs. i (Tl_i is total root length for root branches of order i) for 1759 plants from 77 species (see Appendix E and Table C.1). The vertical bars are the 95% CI. (B) Regression between the theoretical (Eq. (21)) vs. empirical slopes for the relationship ln Tl_i vs. ln r_i for the same data set.

Fig. 13A shows that β and $WBE\,\beta$ become statistically similar for large N. The reason for this convergence is that for large N, $A(N) \to 1$ (Fig. 8), $\varepsilon(N) \to 0.26$ (Eq. (18)), and $n_b \to 1.2$ (Fig. 9B), thus making: $\beta \approx (\frac{1}{1.2*2})^{2*0.26/9} = 0.95$, and $WBE\,\beta = (\frac{1}{1.2})^{1/3} = 0.94$. At low N there is a divergence because β in the WBE model is invariant with N, while in the root model β scales with N (Eq. (18)). Regardless of the divergence, the two are still highly correlated for all N: $R^2 = 0.86$, $P < 0.00001$. The WBE model may be less accurate for small N, because the assumptions of the model are asymptotic in nature and achieved only when $N \to \infty$. The asymptotic convergence between β and $WBE\,\beta$ could potentially be explained by three factors: (1) since r_0 is a power function of N (Eqs. (13) and (17), Fig. 12A), larger N means a larger radius for a substantial part of the root branches; (2) radial conductivity (k_r) is an inverse function of root radius; and (3) larger roots develop a Casparian strip and in some cases a suberized exodermis which can further reduce radial conductivity (Esau, 1965; Peterson, 1988). The combination of these factors would cause larger portions of the root network to behave like a closed network of rigid tubes, and thus follow Murray's scaling laws of $\frac{1}{3}$ (Sherman, 1981; West et al., 1997).

A final point regarding the scaling factor for r and β (Eqs. (12), (16) and (18)). The equations were derived using linear relationships among root radius (r), the average xylem radius (R), and the number of xylem tubes in a bundle (n) (Fig. 2, Table 1). A more generic and flexible equation would have been a power function of the type: $R \approx b_R * r^{b1}$ and $n \approx b_n * r^{b2}$. With a relationship of this type, the generic value for the key scaling factor in Eqs. (12), (16) and (18) would be $\frac{2}{4*b1+b2+3+a}$ instead of the $\frac{2}{8+a}$ for the linear case, where $b1 = b2 = 1$. The improvements derived from the use of a generic power function are marginal for each individual data set in Table 1, and they cancel each other for the combined data set shown in Fig. 2: the R^2 for R vs. r is 0.7 for the power function model vs. 0.64 for the linear one, however for n the R^2's are 0.4 and 0.65, respectively. Taking each

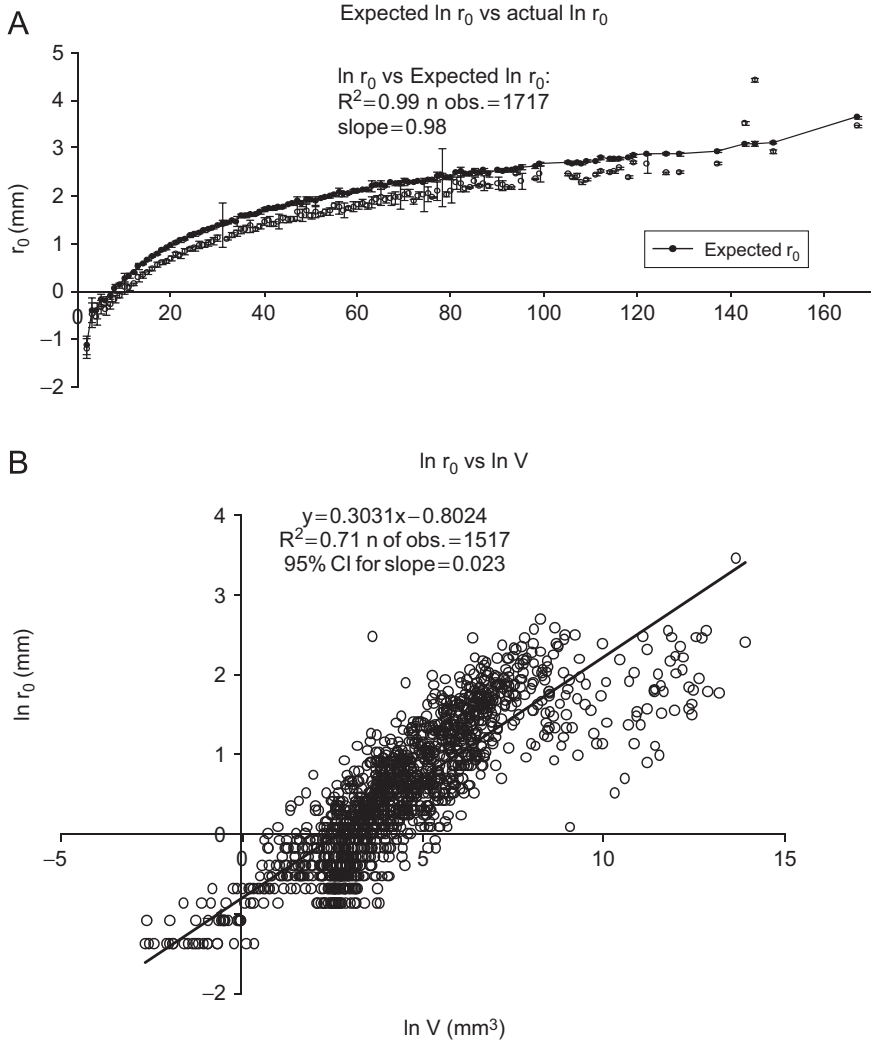

Fig. 12. (A) Actual $\ln r_0$ and expected $\ln r_0$ (the intercept of the regression $\ln r_i$ vs. i) for 1517 plants from 77 species for which there was a complete accounting of root volume (see Appendix C and Table C.1). The vertical bars are the 95% CI. (B) Empirical relationship between $\ln r_0$ and the $\ln V$ for the same data set.

Table 3
Relationships root surface area (RSA), length (RL), root volume (V), and root biomass (RB)

Relationship (Y vs. X)	Equation	R^2	P-value	Slope 95% CI
$\ln RSA$ (mm^2) vs. $\ln V$ (mm^3)	$Y = 3.43 + 0.82 * X$	0.94	0.0001	± 0.020
$\ln RSA$ (mm^2) vs. $\ln RB$ (g)	$Y = 9.88 + 0.92 * X$	0.80	0.0001	± 0.030
$\ln RL$ (mm) vs. $\ln V$ (mm^3)	$Y = 4.10 + 0.76 * X$	0.85	0.0001	± 0.020
$\ln RL$ (mm) vs. $\ln RB$ (g)	$Y = 10.18 + 0.88 * X$	0.76	0.0001	± 0.035

individual data set and calculating the pertinent denominator for the scaling factor ($4 * b1 + b2 + 3$), results in an average value and 95% CI of 8.85 (±1.39). The value of 8 derived from the linear model, thus, is well within this range. The real issue that needs to be seriously addressed is the dearth of data regarding the relationship between root radius, xylem radius, and number of xylem vessels for herbaceous plants (or all plants for that matter). Further improvements in the area of root scaling and water uptake will require more data on this specific area.

To determine if in fact the WBE model is the asymptotic approximation for a root system with large N, we need to look at two other relationships: $\ln Tl_i$ vs. i, and $\ln Tl_i$ vs. $\ln r_i$, where as before Tl_i and r_i are the total root length and radius for root diameter class i. The slope for the $\ln Tl_i$ vs. i in the WBE model is $2/3 * \ln n_b$ (the fractal volume filling assumption). Fig. 13B show the empirical slopes of $\ln Tl_i$ vs. i, and the one calculated by the WBE model. Both slopes are statistically similar for all N. That is not the case for $\ln Tl_i$ vs. $\ln r_i$ because in the WBE model the shape of

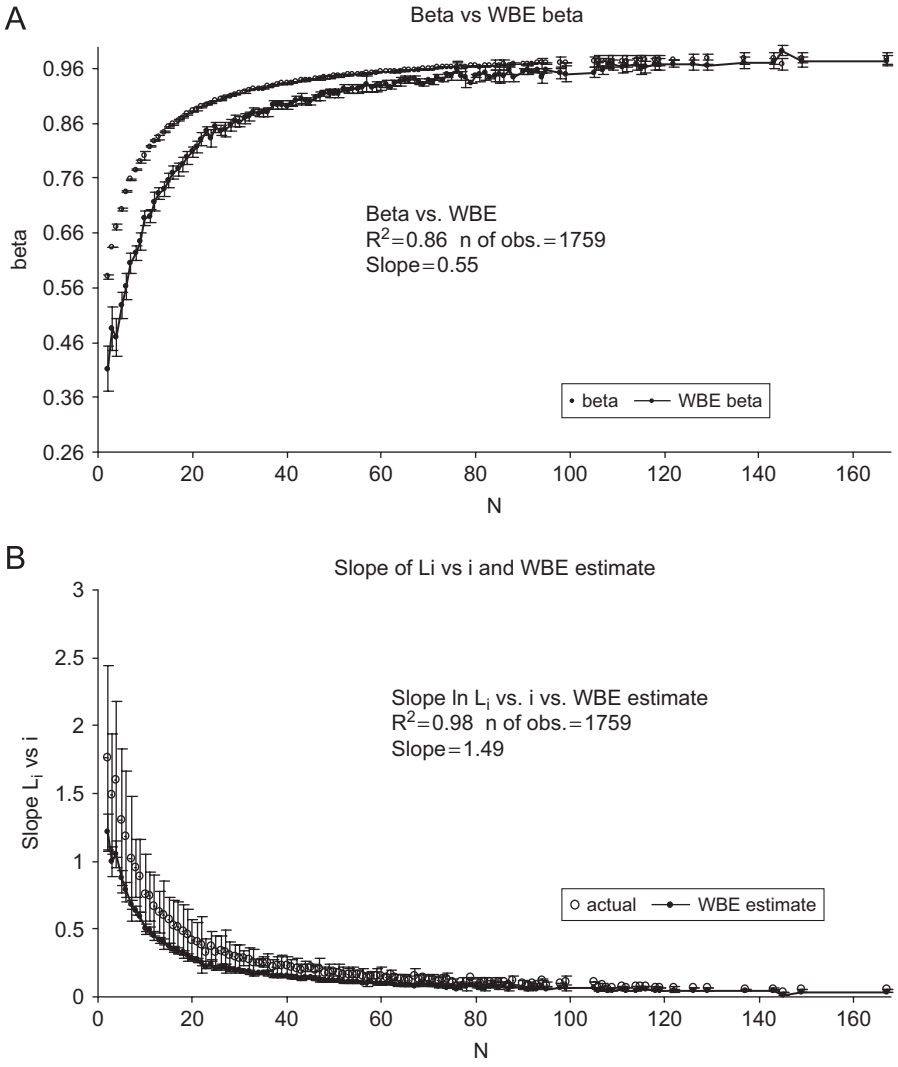

Fig. 13. (A) Empirical β (Fig. 10B) vs. the β from the WBE model for 1759 plants from 77 species (see Appendix C and Table C.1). The vertical bars are the 95% CI. (B) Empirical (Fig. 11B) vs. WBE derives slopes for the relationship between ln Tl_i vs. i (Tl_i is total root length for root branches of order i) for 1759 plants from 77 species (see Appendix C and C.1). The vertical bars are the 95%.

the branching units is preserved (i.e. both length and radius scale as $(1/n_b)^{1/3}$), which leads to a fixed slope of -2 for all N and n_b. In the root model, conversely, the slope is a complex function of both N and n_b (Eq. (21)). Nevertheless, for large N the theoretical slope of the root model (Eq. (21)) also converges to -2. In summary, when all the pieces are put together, it appears that the WBE model is: (a) an asymptotic solution for a root system with large N (and thus biomass); and even more interestingly; (b) that the fractal assumption of volume filling made by West et al. (1997) are also met in the root model (for all N this time), even though they were not explicitly incorporated into it.

The empirical value of $\alpha = 0.3$ for the scaling of r_0 as the function of $V(N)$ (Eq. (17)) is in between the maximum predicted by Eq. (12) (≈ 0.25 for $a \approx 0$) for an open root network, and the $\frac{1}{3}$ predicted by the WBE model (West et al., 1997) for a closed network of rigid tubes (it is $\frac{3}{8}$ in a pulsating system where r_i scales by $\frac{1}{2}$ [West et al., 1997]). To pursue this issue further, I hypothesized that the value for r_0 would be a weighted compromise between the $\frac{1}{3}$ scaling for the above ground xylem system, and the $\frac{2}{9}$ for the root system ($a = 1$). For that purpose I calculated, for each plant, the following weighted average: $\frac{2}{9} * \frac{RB}{TB} + \frac{1}{3} * \frac{AGB}{TB}$ where RB, TB, and AGB are root, total, and above ground biomass. The average across the 1517 plants for which I had a complete accounting of both RB and AGB was 0.3 (± 0.02). While this analysis does not prove it, it at least suggests that r_0 may, in fact, be a compromise between the scaling requirements of an open vs. a close network.

Up to this point all the mathematical derivations involved the assumption of a uniform soil water distribution by depth. In Appendix D, I reanalyze the case of a single root (Fig. 1) when soil water (and thus water pressure) increases exponentially with depth. The solution for water uptake is

$$q(0) = -k_x * \left[\frac{\kappa}{l} * (C_1 - C_2) - \frac{s * \kappa^2 * p(0)}{\kappa^2 - s^2 * l^2}\right], \tag{22}$$

where the constants C_1 and C_2 are defined in Eq. (D.4), $s \geqslant 0$ is a constant, $p(0)$ is soil water pressure at the soil surface (MPa), l is root length (m), and k_x (axial conductivity) and κ are defined in Eqs. (4) and (8). There is no analytical solution for root radius that minimizes Eq. (22) (thus maximizing water uptake) for a fixed root volume (like Eq. (12)). Numerical solutions for a variety of root volumes, however, show that the optimal r for Eq. (22) is very close to the one derived from Eq. (12) (Table D.1). This is not surprising, since Eq. (12) is independent of soil water pressure and water demand. It is thus safe to conjecture that the root scaling that maximizes water uptake (Eqs. (12) and (17)–(19)) is independent of water demand and the actual distribution of soil water (actual water uptake, of course, is not).

Acknowledgments

I am grateful to Jack Norland for providing invaluable help in the design and implementation of the root architecture experiments, to Dr. Thomas Freeman for the information he provided me regarding root anatomy, and to Francis Larson, Dr. Greg Wettstein, and the NDSU CHPC for providing invaluable computing expertise and resources. I am also grateful to two anonymous reviewers whose comments substantially improved this manuscript. Support for this study was provided by grants to the author from the National Science Foundation (DEB-9627928), and USDA-NRICGP (93-0051 and 99-00979).

Appendix A. Optimal radius and length for maximal water flow for a simple one level branching system

The simple branching system (adapted from Roose, 2000) is shown in Fig. 4. Each branch has a root and xylem bundle structure similar to the one shown in Fig. 1. Its total volume (V) is partitioned into V_0 for the main stem and V_1 for the n_b branches (each branch thus has a volume of $1/n_b * V_1$) (Eq. (15)). The radius of the main stem is r, while the radius of each branch is $r_1 = \beta * r$. The length of the main stem is l which is divided into $\lambda * l$ and $(1-\lambda) * l$ $(0<\lambda<1)$ based on the point of insertion of the lateral branches. The length of each of the lateral branches is $l_1 = \gamma * l$. The problem to be solved is as follows: *given a fixed root volume* ($V = V_0 + V_1$), n_b *branches*, *uniform soil water pressure* (p), *and a fixed water pressure at the top of the main stem* (p_0) *find the values for* β *and* γ *the maximize water uptake* ($q[0]$).

A.1. Water pressure within the main stem xylem vessel at $\lambda * l$

To calculate $q(0)$ we first need to calculate the xylem water pressure at $\lambda * l$ ($p_r[\lambda * l]$). For that purpose I divide the main stem into two sections (Fig. 4): (a) the section above the junction with the n_b branches (notation q_{00} for flow, and p_{00r} for pressure) with a length $\lambda * l$ and a volume $\lambda * V_0$; and (b) the one below the junction (notation q_{01} and p_{01r}) with length $(1-\lambda) * l$ and volume $(1-\lambda) * V_0$. Then I solve the following equality:

$$q_{00}(\lambda * l) = q_{01}(0) + n_b q_1(0) = -k_{x00} * \left.\frac{\partial p_{00r}}{\partial z}\right|_{z=\lambda * l} = -k_{x01} * \left.\frac{\partial p_{01r}}{\partial z}\right|_{z=0} - n_b * k_{x1} * \left.\frac{\partial p_{1r}}{\partial z}\right|_{z=0}, \tag{A.1}$$

where q_1 and p_{1r} are water flow rate and pressure in the branches, and the other constants are (using results from Eqs. (4) and (6)):

$$k_{x00} = k_{x01} = \frac{b * \pi * r^5}{8 * \mu}, k_{x1} = \frac{b * \pi * r_1^5}{8 * \mu} = \frac{b * \pi * \beta^5 * r^5}{8 * \mu} = \beta^5 * k_{x00},$$

$$\left.\frac{\partial p_{01r}}{\partial z}\right|_{z=0} = \frac{p_{00r}(\lambda * l) - p}{1 + e^{2 * \kappa_{00}}} * \frac{\kappa_{00}}{(1-\lambda) * l} * (1 - e^{2 * \kappa_{00}}),$$

$$\left.\frac{\partial p_{1r}}{\partial z}\right|_{z=0} = \frac{p_{00r}(\lambda * l) - p}{1 + e^{2\kappa_1}} * \frac{\kappa_1}{\gamma * l} * (1 - e^{2 * \kappa_1}). \tag{A.2}$$

To calculate $\frac{\partial p_{00r}}{\partial z}|_{z=\lambda * l}$ we need to solve Eq. (4) with two fixed boundary conditions (p_0 and $p_{00r}(\lambda * l)$) and then calculate the partial derivative. The result is

$$\left.\frac{\partial p_{00r}}{\partial z}\right|_{z=\lambda * l} = \frac{\kappa_{00}}{\lambda * l * (e^{\kappa_{00}} - e^{-\kappa_{00}})} * [(p_{00r}(\lambda * l) - p) * (e^{\kappa_{00}} + e^{-\kappa_{00}}) + 2 * (p - p_0)]. \tag{A.3}$$

Putting together Eqs. (A.1)–(A.3), we can now solve for $p_{00r}(\lambda * l)$:

$$p_{00r}(\lambda * l) = p - \frac{B_{00} * (p - p_0)}{A_{00} - A_{01} - n_b * \beta^5 * A_1},$$

$$A_{00} = \frac{\kappa_{00}}{\lambda * l} * \frac{e^{\kappa_{00}} + e^{-\kappa_{00}}}{e^{\kappa_{00}} - e^{-\kappa_{00}}},$$

$$A_{01} = \frac{\kappa_{01}}{(1-\lambda) * l} * \frac{1 - e^{2*\kappa_{01}}}{1 + e^{2*\kappa_{01}}},$$

$$A_1 = \frac{\kappa_1}{\gamma * l} * \frac{1 - e^{2*\kappa_1}}{1 + e^{2*\kappa_1}},$$

$$B_{00} = \frac{2 * \kappa_{00}}{\lambda * l * (e^{\kappa_{00}} - e^{-\kappa_{00}})}. \tag{A.4}$$

With the use of the definition for κ from Eqs. (4) and (8) we can calculate κ_{00}, κ_{01}, and κ_1 as

$$\kappa_{00} = 4 * r^{-\frac{1}{2}(4+a)} * \sqrt{\frac{k_{r0} * r0^a * \mu}{b}} * \lambda * l,$$

$$\kappa_{01} = \frac{1-\lambda}{\lambda} * \kappa_{00},$$

$$\kappa_1 = \frac{\beta^{-\frac{1}{2}(4+a)} * \gamma}{\lambda} * \kappa_{00}. \tag{A.5}$$

A.2. Water uptake

Water uptake is calculated by

$$q_{00}(0) = -k_{x00} * \left.\frac{\partial p_{00r}}{\partial z}\right|_{z=0}.$$

The partial derivative can be calculated by the same procedure used to calculate $k_{x00} * \frac{\partial p_{00r}}{\partial z}|_{z=\lambda * l}$. The result is

$$q_{00}(0) = -k_{x00} * \left.\frac{\partial p_{00r}}{\partial z}\right|_{z=0} = -\frac{k_{x00} * \kappa_{00}}{\lambda * l} * \frac{2 * (p_{00r}(\lambda * l) - p) + (p - p_0) * (e^{\kappa_{00}} + e^{-\kappa_{00}})}{e^{\kappa_{00}} - e^{-\kappa_{00}}}. \tag{A.6}$$

Using Eq. (A.4), then we have that

$$q_{00}(0) = \frac{D * (p - p_0)}{EN} * \left(\frac{-4 * C_1}{EP * C_1 - \left(1 - e^{\frac{2*(1-\lambda)*\kappa_{00}}{\lambda}}\right) * C_2 - n_b * \beta^{\frac{6-a}{2}} * \left(1 - e^{\frac{2*\gamma*\kappa_{00}}{\lambda * \beta^{\frac{4+a}{2}}}}\right) * C_3} + EP \right), \tag{A.7}$$

where

$$D = -\frac{b * \pi * \sqrt{\frac{k_{r0} * r0^a}{b}}}{2 * \sqrt{\mu}} * r^{\frac{6-a}{2}}, \quad EP = e^{\kappa_{00}} + e^{-\kappa_{00}}, \quad EN = e^{\kappa_{00}} - e^{-\kappa_{00}}$$

and

$$C_1 = \left(1 + e^{\frac{2*(1-\lambda)*\kappa_{00}}{\lambda}}\right) * \left(1 + e^{\frac{2*\gamma*\kappa_{00}}{\lambda * \beta^{\frac{4+a}{2}}}}\right),$$

$$C_2 = EN * \left(1 + e^{\frac{\frac{2*\gamma*\kappa_{00}}{\lambda}}{\beta^{\frac{4+a}{2}}}}\right),$$

$$C_3 = EN * \left(1 + e^{\frac{2*(1-\lambda)*\kappa_{00}}{\lambda}}\right).$$

A.3. Maximizing water uptake

The objective is to minimize Eq. (A.7) (uptake is a negative number) with the following constraint:

$$\pi * r^2 * l + n_b * \pi * (\beta * r)^2 * \gamma * l = V \Rightarrow \pi * r^2 * l * (1 + n_b * \beta^2 * \gamma) - V = 0. \tag{A.8}$$

For that purpose I use Lagrange multipliers (Riley et al., 2002, p. 171) which requires the solving of this system of equations:

$$\frac{\partial q_{00}(0)}{\partial \beta} - 2 * n_b * \beta * \gamma * \pi * r^2 * l = 0,$$

$$\frac{\partial q_{00}(0)}{\partial \gamma} - n_b * \beta^2 * \pi * r^2 * l = 0 \tag{A.9}$$

which are

$$\frac{n_b * \pi * b * e^{2*\kappa_{00}} * \left(1 + e^{2*\kappa_{00}*(\frac{1}{\lambda}-1)}\right)^2 * \sqrt{\frac{k_{r0} * r0^a}{b}} * (p - p_0) * r^{3-\frac{a}{2}}}{(e^{-2*\kappa_{00}} * (e^{2*\kappa_{00}} - 1) * \left(e^{2*\kappa_{00}} + e^{\frac{2*\kappa_{00}}{\lambda}}\right) * (e^{X(\beta,\gamma)} - 1) * n_b * \beta^3 + 2 * \left(1 + e^{\frac{2*\kappa_{00}}{\lambda}}\right) * (1 + e^{X(\beta,\gamma)}) * \beta^{\frac{a}{2}})^2 * \sqrt{\mu} * \lambda$$
$$* (4 * (4 + a) * e^{X(\beta,\gamma)} * \kappa_{00} * \gamma + (6 - a) * \beta^{\frac{4+a}{2}} * \lambda * (1 - e^{2*X(\beta,\gamma)})) - 2 * n_b * \beta * \gamma * \pi * r^2 * l = 0 \tag{A.10}$$

and

$$\frac{8 * n_b * \pi * \beta * b * e^{2*\kappa_{00}} * e^{X(\beta,\gamma)} * \left(1 + e^{2*\kappa_{00}*(\frac{1}{\lambda}-1)}\right)^2 * \kappa_{00} * \sqrt{\frac{k_{r0} * r0^a}{b}} * (p - p_0) * r^{3-\frac{a}{2}}}{(e^{-2*\kappa_{00}} * (e^{2*\kappa_{00}} - 1) * \left(e^{2*\kappa_{00}} + e^{\frac{2*\kappa_{00}}{\lambda}}\right) * (e^{X(\beta,\gamma)} - 1) * n_b * \beta^3 + 2 * \left(1 + e^{\frac{2*\kappa_{00}}{\lambda}}\right) * (1 + e^{X(\beta,\gamma)}) * \beta^{\frac{a}{2}})^2 * \sqrt{\mu} * \lambda$$
$$- n_b * \beta^2 * \pi * r^2 * l = 0, \tag{A.11}$$

where

$$X(\beta, \gamma) = \frac{2 * \kappa_{00} * \beta^{-\frac{4+a}{2}} * \gamma}{\lambda}. \tag{A.12}$$

Since Eqs. (A.10) and (A.11) share a denominator, they can be manipulated and simplified to the following equality:

$$e^{2*X(\beta,\gamma)} = 1 - \frac{2 * (8 + a)}{a - 6} * X(\beta, \gamma) * e^{X(\beta,\gamma)}. \tag{A.13}$$

As the reader will notice, this is the same as Eq. (11) except that X is a function of β and γ. As was the case with Eq. (11), (A.13) has numerical solutions for $0 < a < 6$. It can be shown that the solution for Eq. (A.13) is also the minimum for (A.7).

A.4. Values of β and γ that maximize water uptake

We need to find the values for β and γ that solve $X(\beta, \gamma) = C$, where C is the solution to Eq. (A.13) (for example for $a = 1$, $C = 1.9861$). We can now use Eqs. (15) and (A.8) to make γ a function of β:

$$\pi * r^2 * l * (1 + n_b * \beta^2 * \gamma) = V_0 * (1 + n_b * \beta^2 * \gamma) = V = V_0 * (1 + A(N))$$
$$\Rightarrow \gamma = \frac{A(N)}{n_b} * \beta^{-2}. \tag{A.14}$$

From (A.5) we have that

$$\kappa_{00} = 4 * r^{-\frac{1}{2}(4+a)} * \sqrt{\frac{k_{r0} * r0^a * \mu}{b}} * \lambda * l = 4 * r^{-\frac{1}{2}(4+a)} * \sqrt{\frac{k_{r0} * r0^a * \mu}{b}} * \lambda * \frac{V_0}{\pi * r^2}$$

$$\Rightarrow \kappa_{00} = 4 * \lambda * \frac{V_0}{\pi} * \sqrt{\frac{k_{r0} * r0^a * \mu}{b}} * r^{-\frac{1}{2}(8+a)}. \tag{A.15}$$

Finally the value for r scales with V as defined in Eq. (12). We can now use the solution to Eq. (A.12) to find β as

$$\frac{2 * \kappa_{00} * \beta^{-\frac{4+a}{2}} * \gamma}{\lambda} = \frac{8 * \lambda * \frac{V_0}{\pi} * \sqrt{\frac{k_{r0} * r0^a * \mu}{b}} * r^{-\frac{1}{2}(8+a)} * \beta^{-\frac{4+a}{2}} * \frac{A(N)}{n_b} * \beta^{-2}}{\lambda} = C$$

$$\Rightarrow 8 * \frac{V_0}{\pi} * \sqrt{\frac{k_{r0} * r0^a * \mu}{b}} * \left[\left(\frac{8 * V_0 * (1 + A(N)) \sqrt{\frac{k_{r0} r0^a \mu}{b}}}{\pi C} \right)^{\frac{2}{8+a}} \right]^{-\frac{1}{2}(8+a)} \frac{A(N)}{n_b} * \beta^{-\frac{8+a}{2}} = C$$

$$\Rightarrow \beta = \left(\frac{A(N)}{n_b * (1 + A(N))} \right)^{\frac{2}{8+a}}. \tag{A.16}$$

A final note, as with the case of r (Eq. (12)), the optimal β is also independent of soil water pressure (p) and water demand (p_0).

Appendix B. A model for a root branching network and some of its scaling properties

B.1. Water flow functions for the root branching network

The objective is to model water uptake and flow for a network of the type shown in Fig. 6 with the volume distribution, number of branches per root node, and the scaling radius and length at each node defined by Eqs. (13), (17)–(19). The equivalent values for Eqs. (A.4)–(A.5) are as follows:

$$\kappa_{0i} = \frac{4 * \lambda * V_i * \sqrt{\frac{k_{r0} * r0^a * \mu}{b}}}{n_b^i * \pi * r_i^{\frac{8+a}{2}}},$$

$$\kappa_{1i} = \frac{4 * (1 - \lambda) * V_i * \sqrt{\frac{k_{r0} * r0^a * \mu}{b}}}{n_b^i * \pi * r_i^{\frac{8+a}{2}}},$$

$$\kappa_N = \frac{4 * V_N * \sqrt{\frac{k_{r0} * r0^a * \mu}{b}}}{n_b^i * \pi * r_N^{\frac{8+a}{2}}}, \tag{B.1}$$

$$A_{0,i} = \frac{\kappa_{0,i}}{l_{0,i}} * \frac{e^{\kappa_{0,i}} + e^{-\kappa_{0,i}}}{e^{\kappa_{0,i}} - e^{-\kappa_{0,i}}},$$

$$A_{1,i} = \frac{\kappa_{1,i}}{l_{1,i}} * \frac{1 - e^{2*\kappa_{0,i}}}{1 + e^{2*\kappa_{0,i}}},$$

$$A_N = \frac{\kappa_N}{l_N} * \frac{1 - e^{2*\kappa_N}}{1 + e^{2*\kappa_N}},$$

$$B_{0,i} = \frac{\kappa_{0,i}}{l_{0,i}} * \frac{2}{e^{\kappa_{0,i}} - e^{-\kappa_{0,i}}}. \tag{B.2}$$

The values from Eqs. (B.1)–(B.2) can then be used to calculate water pressure at each junction between roots of order i and $i+1$ as follows:

$$D_{(N\times 1)} = \begin{bmatrix} \dfrac{p*((A_{0,0}-A_{1,0})*r_0^5+n_b*A_{0,1}*r_1^5-B_{0,0}*r_0^5-n_b*B_{0,1}*r_1^5)+p_0*B_{0,0}*r_0^5}{(A_{0,0}-A_{1,0})*r_0^5+n_b*A_{0,1}*r_1^5} \\ \dfrac{p*((A_{0,1}-A_{1,1})*r_1^5+n_b*A_{0,2}*r_2^5-B_{0,1}*r_1^5-n_b*B_{0,2}*r_2^5)}{(A_{0,1}-A_{1,1})*r_1^5+n_b*A_{0,2}*r_2^5} \\ \cdots\cdots\cdots \\ \dfrac{p*((A_{0,N-2}-A_{1,N-2})*r_{N-2}^5+n_b*A_{0,N-1}*r_{N-1}^5-B_{0,N-2}*r_{N-2}^5-n_b*B_{0,N-1}*r_{N-1}^5)}{(A_{0,N-2}-A_{1,N-2})*r_{N-2}^5+n_b*A_{0,N-1}*r_{N-1}^5} \\ \dfrac{p*((A_{0,N-1}-A_{1,N-1})*r_{N-1}^5+n_b*A_{0,N}*r_N^5-B_{0,N-1}*r_{N-1}^5)}{(A_{0,N-1}-A_{1,N-1})*r_{N-1}^5+n_b*A_{0,N}*r_N^5} \end{bmatrix}, \tag{B.3}$$

$$dleft_i = \frac{-B_{0,i}*r_i^5}{(A_{0,i}-A_{1,i})*r_i^5+n_b*A_{0,i+1}*r_{i+1}^5},$$

$$dright_i = \frac{-n_b*B_{0,i+1}*r_{i+1}^5}{(A_{0,i}-A_{1,i})*r_i^5+n_b*A_{0,i+1}*r_{i+1}^5},$$

$$dleft_{N-1} = \frac{-B_{0,N-1}*r_{N-1}^5}{(A_{0,N-1}-A_{1,N-1})*r_{N-1}^5+n_b*A_{0,N}*r_N^5},$$

$$E_{(N\times N)} = \begin{bmatrix} 1 & dright_0 & & \\ dleft_1 & 1 & dright_1 & \\ . & . & . & . \\ . & . & dleft_{N-1} & 1 \end{bmatrix},$$

$$P_{(N\times 1)} = \begin{bmatrix} p_0(\lambda*l_{0,0}) \\ p_1(\lambda*l_{0,1}) \\ \cdots\cdots \\ p_i(\lambda*l_{0,i}) \\ \cdots\cdots \\ p_{N-1}(\lambda*l_{0,N-1}) \end{bmatrix} = E^{-1}.D, \tag{B.4}$$

where $p_i(\lambda*l_{0,i})$ is the water pressure in xylem bundle i at its junction with the n_b roots of $i+1$ (Fig. 6). With the pressure data calculated in (B.4), we can now estimate water uptake by the root network using Eq. (A.6):

$$q_0(0) = -\frac{b*\pi*r_0^5}{8*\mu}*\frac{\kappa_{00}}{\lambda*l_{00}}*\frac{2*(p_{0r}(\lambda*l_{00})-p)+(p-p_0)*(e^{\kappa_{00}}+e^{-\kappa_{00}})}{e^{\kappa_{00}}-e^{-\kappa_{00}}}. \tag{B.5}$$

An example on the use of these equations follows. The parameters for the root volume equations (Eq. (13)) are: $N=7$; $n_b=2$; $v_0=2.0*10^{-12}$ (m^3); $\delta_0=2.0828$; $\eta=4.7407$; $\rho=1.0037$. The additional parameters for Eqs. (17)–(19), and (B.1)–(B.5) are: $\mu=1.01*10^{-9}$ (MPa s); $k_{r0}=2.5*10^{-7}$ (m s^{-1} MPa^{-1}); $r_0=5*10^{-4}$ (m); $r_c=3.95*10^{-5}$ (m);

$b = b_n * b_R^4 = 0.02728\,(\mathrm{m}^{-1})$; $\lambda = 0.2$; $\alpha = 2/9$; $a = 1$; $C = 1.9861$; $p = -3\,(\mathrm{MPa})$; $p_0 = -12\,(\mathrm{MPa})$.

$$D = \begin{bmatrix} -6.86842 \\ -0.0000905227 \\ -0.000792219 \\ -0.00691174 \\ -0.0587283 \\ -0.412589 \\ -1.78417 \end{bmatrix},$$

$$E = \begin{bmatrix} 1 & -0.427624 & 0 & 0 & 0 & 0 & 0 \\ -0.732193 & 1 & -0.267777 & 0 & 0 & 0 & 0 \\ 0 & -0.732035 & 1 & -0.267701 & 0 & 0 & 0 \\ 0 & 0 & -0.730658 & 1 & -0.267038 & 0 & 0 \\ 0 & 0 & 0 & -0.719003 & 1 & -0.261421 & 0 \\ 0 & 0 & 0 & 0 & -0.63997 & 1 & -0.222494 \\ 0 & 0 & 0 & 0 & 0 & -0.405248 & 1 \end{bmatrix},$$

$$P = E^{-1}.D = \begin{bmatrix} -11.9597 \\ -11.9060 \\ -11.7600 \\ -11.3697 \\ -10.3737 \\ -8.18671 \\ -5.10206 \end{bmatrix},$$

$$q(0) = -1.48 * 10^{-9}\,(\mathrm{m}^3\,\mathrm{s}^{-1}). \tag{B.6}$$

B.2. Scaling of root length vs. root radius and root order

Total root length at root node i (Tl_i) can be calculated from Eqs. (13) and (18) as

$$Tl_i = n_b * (l_{0,i} + l_{1,i}) = \frac{V_i}{\pi * r_i^2} = \frac{V_0(N) * (1 - A(N)^{-1})}{r_0(N)^2 * \pi} * \left(n_b^{\frac{4*\varepsilon(N)}{8+a}} * A(N)^{\frac{8+a-4*\varepsilon(N)}{8+a}} * (1 + A(N))^{\frac{4*\varepsilon(N)}{8+a}} \right)^i. \tag{B.7}$$

From Eq. (18) we can calculate the value of i as a function of r_i as

$$\begin{aligned} \ln r_i(N) &= \ln r_0(N) + i * \frac{2 * \varepsilon(N)}{8 + a} * \ln\left(\frac{A(N)}{n_b * (1 + A(N))}\right) \\ \Rightarrow i &= \frac{\ln r_i - \ln r_0(N)}{\frac{2 * \varepsilon(N)}{8 + a} * \ln\left(\frac{A(N)}{n_b * (1 + A(N))}\right)}. \end{aligned} \tag{B.8}$$

Combining Eqs. (B.7)–(B.8) we can calculate the scaling of Tl_i as a function of root node (i) and root radius (r_i)

$$\ln Tl_i(N) \approx \frac{\ln\left(n_b^{\frac{4*\varepsilon(N)}{8+a}} * A(N)^{\frac{8+a-4*\varepsilon(N)}{8+a}} * (1 + A(N))^{\frac{4*\varepsilon(N)}{8+a}} \right)}{\frac{2 * \varepsilon(N)}{8 + a} * \ln\left(\frac{A(N)}{n_b * (1 + A(N))}\right)} * \ln r_i. \tag{B.9}$$

B.3. Scaling of root length and root surface area as a function of V

We can calculate root surface area (RSA in m^3), and root length (RL in m) as a function of $V(N)$ as follows:

$$\begin{aligned} RSA &= 2*\pi*r_0*\left[l_0+\sum_{i=1}^{N-1} n_b^i*\beta^i*(l_{0,i}+l_{1,i})+n_b^N*\beta^N*l_N\right] \\ &= \frac{2*V_0(N)}{rconst*V(N)^{\alpha}} \\ &\quad *\left(1+\frac{(A(N)-1)*(rconst*V_0(N)^{\alpha})^{\frac{1}{N}}*\left(\left(\frac{A(N)^{1+\alpha}*(rconst*V_0(N)^{\alpha})^{\frac{1}{N}}}{rc^{\frac{1}{N}}}\right)^N-1\right)}{A(N)*(rconst*V_0(N)^{\alpha})^{\frac{1}{N}}-\frac{rc^{\frac{1}{N}}}{A(N)^{\alpha}}}\right), \end{aligned} \tag{B.10}$$

$$\begin{aligned} RL &= l_0+\sum_{i=1}^{N-1} n_b^i*(l_{0,i}+l_{1,i})+n_b^N*l_N \\ &= \frac{V_0(N)}{\pi*rconst^2*V(N)^{2*\alpha}} \\ &\quad *\left(1+\frac{(A(N)-1)*(rconst*V_0(N)^{\alpha})^{\frac{2}{N}}*\left(\left(\frac{A(N)^{1+2*\alpha}*(rconst*V_0(N)^{\alpha})^{\frac{2}{N}}}{rc^{\frac{2}{N}}}\right)^N-1\right)}{A(N)*(rconst*V_0(N)^{\alpha})^{\frac{2}{N}}-\frac{rc^{\frac{2}{N}}}{A(N)^{2*\alpha}}}\right). \end{aligned} \tag{B.11}$$

$V(N)$, $A(N)$, and $V_0(N)$ are dependent on N as defined in Eq. (13). Both RSA and RL are complex function of N, but upper bound of the slopes of the regression $\ln RSA$ vs. $\ln V$ and $\ln RL$ vs. $\ln V$ is 1.

Appendix C. Root measurements

Root measurements were conducted on 1759 plants from the 77 species shown in Table C.1. The measurements consisted of: (1) number of root diameter classes (N); (2) the diameter of each diameter class ($2*r_i$); (3) number of root branches per diameter class (N_i); (4) the root length, surface area, and volume per each diameter class; and (5) total aboveground and root biomass. The measurements were derived from four experiments: two greenhouse experiments, a large box outdoor experiment, and a field experiment. The experiments were designed to track the root development of plant species from the juvenile stage (45–60 days) to the adult stage (1–2 growing seasons), and to cover a large range of biomass, growing conditions, and nutrient levels.

Detailed methodologies for the greenhouse experiments have already been reported in Johnson and Biondini (2001) and Levang-Brilz and Biondini (2002). The large box experiment was similar in design to the greenhouse experiments, except that it was conducted outside the greenhouse using $1\times1\times1$ m wooden boxes equipped with detachable sides and filled with washed river sand. The boxes had three 2 cm^2 hardware mesh panels inserted horizontally at depths of 10, 30, and 60 cm. The mesh was intended to keep the roots in place after the sand had been removed. Two treatments were used: (1) no fertilization; and (2) fertilization with Sierra® slow release fertilizer prills (N-P-K:16-8-12 plus minor nutrients) at a rate of 37.5 g N m^{-2}. Each treatment was replicated 5 times. Plants were grown for an entire growing season and harvested in October. The harvesting and root measurements were the same as in Levang-Brilz and Biondini (2002).

The field experiments were conducted at NDSU Albert Ekre Grassland Preserve, in south eastern ND. The soils in the experimental site belong to the Embden-Tiffany fine sandy loam series. The soils are of moderate fertility, have 0–3% slope, are moderately well drained, and have a combined A&B horizon of approximately 69 cm. The advantage of this experiment was that it allowed us to examine roots grown under normal field conditions, and provided two growing seasons of root development. The disadvantage is that the root system information needed to be acquired by root coring. Thus, unlike the previous experiments, the entire root system could not be measured and its total biomass (and thus volume) were unaccounted.

Table C.1
List of species used in the root experiments. Nomenclature and authorities follows the Great Plains Flora Association (1986)

Forbs/Sedges/Shrubs			
Achillea millefolium L.	*Chenopodium album* L.	*Helianthus maximilliana* Schrad.	*Rosa arkansana* Porter
Agoseris glauca (Pursh Dietr.)	*Chrysopsis villosa* (Pursh) Nutt.	*Helianthus rigidus* (Cass.) Desf.	*Rudbeckia hirta* L.
Allium stellatum Ker.	*Cirsium arvense* L.	*Heuchera richardsonii* R. Br.	*Rumex crispus* L.
Amaranthus retroflexus L.	*Conyza Canadensis* (L.) Cronq.	*Liatris punctata* Hook.	*Solidago missouriensis* Nutt.
Amorpha canescens Pursh	*Coreopsis lanceolata* L.	*Linum perenne* L.	*Solidago rigida* L.
Anaphalis margaritacea (L.) Benth. & Hook.	*Dalea purpurea* Vent.	*Lupinus perennis* S. Wats. [legume]	*Sonchus arvensis* L.
Artemisia dracunculus L.	*Erigeron philadelphicus* L.	*Melilotus officinalis* L.	*Sphaeralcea coccinea* (Pursh) Rydb.
Artemisia frigida Willd.	*Erysimum asperum* (Nutt.) DC.	*Oenothera biennis* L.	*Taraxacum officinale* Weber
Artemisia ludoviciana Nutt.	*Gaillardia aristata* Pursh	*Opuntia fragilis* (Nutt.) Haw.	*Tragopogon dubiusI* Scop.
Artemisia tridentata Nutt.	*Galium boreale* L.	*Oxytropis lambertii* Pursh.	*Verbena stricta* Vent.
Asclepias verticillata L.	*Geum triflorum* Pursh	*Plantago major* L.	*Vicia americana* Muhl. ex Willd
Aster ericoides L.	*Grindelia squarrosa* Pursh	*Potentilla pennsylvanica* L.	*Viola pedatifida* G. Don
Astragalus Canadensis L.	*Haplopappus spinulosus* (Pursh) DC.	*Potentilla arguta* Pursh.	
Campanula rotundifolia L.	*Hedeoma* hispida	*Psoralea esculenta* Pursh.	
Carex heliophila Mack.	*Helianthus maximilianii* Schrad.	*Ratibida columnifera* (Nutt.) Woot. & Standl.	
Grasses			
Agropyron cristatum (L.) Gaertn.	*Bouteloua curtipendula* (Michx.) Torr.	*Elymus canadensisI* L.	*Schizachyrium* scoparium (Michx.) Nash-Gould
Agropyron repens (L.) Beauv.	*Bouteloua gracilis* (H.B.K.) Lag. ex Griffiths	*Hordeum jubatum* L.	*Sorghastrum nutans* L.
Aropyron smithii Rybd.	*Bromus inermis* Leyss.	*Koeleria cristata* (Lam.) Beauv.	*Sporobolus cryptandrus* (Torr.) A. Gray
Agropyron spicatum (Pursh) Scribn. & Sm.	*Bromus tectorum* L.	*Panicum virgatum* L.	*Stipa comata* Trin. & Rupr.
Andropogon gerardii Vitman	*Calamovilfa longifolia* (Hook) Scribn.	*Poa pratensis* L.	*Stipa viridula* Trin.

The field design for the non-rhizomatous species of Table C.1 consist of a 88 m by 48 m plots, covered with a garden type cloth, in which openings had been made, in a grid fashion, at 4 m intervals to transplant the plants under study. The 4 m spacing between transplants was designed to minimize the intermingling of roots among plants so there was a high probability of associating root core data with the target plant (see below for details). The garden cloth was used to prevent the establishment of unwanted species in the open spaces between the plants under study (the cloth allowed for air and water to freely circulate but was impenetrable by light). Five plants per species were randomly transplanted in the openings in the cloth during the summer of year 1 and harvested in the fall of year 2. At harvest time above ground biomass was clipped at the surface level, and three soil cores (10 cm in diameter) were taken in the following manner: (a) a core was taken at the center of the plant; and (b) two cores were taken covering the distance of 5–25, and 25–50 cm from the center of the plant. All the cores were taken to a depth of 0.5 m and subdivided into three intervals: 0–10 cm, 10–20 cm, and 20–50 cm. After extraction, the soil cores were manually washed to remove the soil material. Root measurements were made using the same methodology of Levang-Brilz and Biondini (2002). Above-ground and root biomass (by core and depth) were dried at 60 °C for 72 h and weighed.

For the experiment involving the three strongly rhizomatous species (*Agropyron repens*, *Agropyron smithii*, and *Artemisia ludoviciana*) garden cloth could not be used since it would have prevented the emergence of new shoots from the rhizomes. Consequently, we tilled a 34 × 34 m area and kept it black for a 2 year period with periodic re-tilling. The purpose of this treatment was to reduce, as much as possible, the seed bank. Five plants per species, with an 8 m spacing between plants were planted in the center 31 × 31 m section of the plot. The 8 m spacing was designed to minimize the intermingling of roots among plants so there was a high probability of associating root core data with the target plant. All plants not belonging to the target species were manually removed throughout the growing season. Plants were harvested in October. Above-ground biomass was clipped at the surface level and, depending on rhizome extension, a maximum of 12 soil cores (10 cm in diameter) were taken along the direction of the rhizomes. All the cores were taken to a depth of 0.5 m and subdivided into three intervals: 0–10 cm, 10–20 cm, and 20–50 cm. Above-ground biomass and soil cores were processed as described above.

Table D.1
Example of optimization of root radius for maximum water uptake for a single root for the case of a uniform (Eq. (9)) vs. an exponential water distribution (Eq. (22))

Root volume (m^2)	Uniform soil water distribution		Exponential soil water distribution	
	Radius (m)	Water uptake ($m^3\,s^{-1}$)	Radius (m)	Water uptake ($m^3\,s^{-1}$)
$1.57*10^{-6}$	$6.43*10^{-4}$	$6.530*10^{-9}$	$6.40*10^{-4}$	$6.240*10^{-9}$
$1.57*10^{-7}$	$3.85*10^{-4}$	$1.817*10^{-9}$	$3.83*10^{-4}$	$1.791*10^{-9}$
$1.57*10^{-8}$	$2.31*10^{-4}$	$5.056*10^{-10}$	$2.30*10^{-4}$	$5.037*10^{-10}$

The parameter used were $a=1$, $k_{r0}=2.5*10^{-7}$, $r_0=5*10^{-4}$, $b=b_n*b_R^4=0.02728$, $s=3$, $p_0=-12$ (see text and Appendix D for definitions). For the case of a uniform water distribution soil water potential was set at $p=-3$ at all depths. In the case of an exponential water distribution (Eq. (22)), $p(0)$ was set up so that the integrated amount of water available to the root was the same for both cases.

Appendix D. Optimal root radius for water uptake for an un-even distribution of soil water

In the case of the single root system I derived the optimal root radius that maximizes water uptake for a fixed root volume and uniform soil water pressure (Eqs. (1)–(12)). Here I reanalyze the same problem by relaxing the second condition and assuming that soil water (and thus water pressure) increases exponentially with depth:

$$p(z)=e^{-s*z}*p(0),\quad 0\leqslant z\leqslant l \text{ and } s\geqslant 0, \tag{D.1}$$

where z (m) is depth ($z=0$ at the top of the root), s is a constant, $p(0)$ is soil water pressure at the soil surface (MPa), and l is root length (m). To determine the water pressure (MPa) within xylem vessels (p_r) we need to solve an equation similar to Eq. (3), which in this case is

$$\frac{\partial^2 p_r(z)}{\partial z^2}=\frac{2*\pi*r*k_r}{k_x}*(p_r(z)-e^{-s*z}*p(0)), \tag{D.2}$$

where k_r is the radial conductivity, k_x (axial conductivity) and κ are defined in Eqs. (4) and (8), and r is the root radius (m). The solution to (D.2) is

$$p_r(z)=C_1*e^{\frac{\kappa}{l}*z}+C_2*e^{-\frac{\kappa}{l}*z}+\frac{\kappa^2*e^{-s*z}*p(0)}{\kappa^2-s^2*l^2}, \tag{D.3}$$

where C_1 and C_2 are constants that depend on the boundary condition. For boundary conditions $p_r(0)=p_0$, and $\frac{\partial p_r}{\partial z}|_{z=l}=0$, the C_1 and C_2 are constants are

$$C_1=\frac{e^{-\kappa}*[(\kappa^2-s^2*l)*p_0-\kappa^2*p(0)]+\kappa*l*s*e^{-s*l}*p(0)}{(\kappa^2-s^2*l)*(e^{\kappa}+e^{-\kappa})},$$

$$C_2=\frac{e^{\kappa}*[(\kappa^2-s^2*l)*p_0-\kappa^2*p(0)]-\kappa*l*s*e^{-s*l}*p(0)}{(\kappa^2-s^2*l)*(e^{\kappa}+e^{-\kappa})}. \tag{D.4}$$

For the case of $s=0$ (uniform distribution of soil water), Eq. (D.3) reduces to Eq. (5).

Root water uptake then is

$$q(0)=-k_x*\left.\frac{\partial p_r}{\partial z}\right|_{z=0}=-k_x*\left[\frac{\kappa}{l}*(C_1-C_2)-\frac{s*\kappa^2*p(0)}{\kappa^2-s^2*l^2}\right]. \tag{D.5}$$

Unlike the case of a uniform soil water pressure, there is no analytical solution (like Eq. (12)) for the r that minimizes (D.5) (thus maximizing water uptake). In the Discussion section, I show that numerical solutions for r that minimize (D.5) are very similar to the one provided by Eq. (12) (Table D.1).

Appendix E. Supplementary data

Supplementary data associated with this article can be found in the online version at doi:10.1016/j.jtbi.2007.11.018.

References

Bejan, A., 1997. Advanced Engineering Thermodynamics, second ed. Wiley, New York.

Bejan, A., 2000. Shape and Structure, from Engineering to Nature. Cambridge University Press, UK.

Biondini, M., 2001. A three dimensional spatial model for plant competition in an heterogeneous soil environment. Ecol. Modeling 142, 189–225.

Brown, J.H., Enquist, B.J., West, G.B., 1998. Allometric scaling in biology. Science 281, 752–753.

Brown, J.H., West, G.B., Enquist, B.J., 2000. In: Brown, J.H., West, G.B. (Eds.), Scaling in Biology: Patterns, Processes, Cause, and Consequences. Scaling in Biology. Oxford University Press, Oxford, pp. 1–24.

Brown, J.H., West, G.B., Enquist, B.J., 2005. Yes, West, Brown and Enquist's model of allometric scaling is both mathematically correct and biologically relevant. Funct. Ecol. 19, 735–738.

Dawson, T.H., 1998. Allometric scaling in biology. Science 281, 751–752.

Dodds, P.S., Rothman, D.H., Weitz, J.S., 2001. Re-examination of the "3/4-law" of metabolism. J. Theor. Biol. 209, 9–27.

Esau, K., 1965. Plant Anatomy, second ed. Wiley, New York.

Fitter, A.H., 1987. An architectural approach to the comparative ecology of plant root systems. New Phytol. 106, 61–77.

Great Plains Flora Association, 1986. Flora of the Great Plains. University Press of Kansas, Lawrence, Kansas.

Hacke, U.G., Sperry, J.S., 2001. Functional and ecological xylem anatomy. Perspect. Ecol. Evolution Systematics 4, 97–155.

Huang, B., Eissenstat, D.M., 2000. Linking hydraulic conductivity to anatomy in plants that vary in specific root length. J. Am. Soc. Horticultural Sci. 125, 260–264.

Johnson, H., Biondini, M.E., 2001. Root morphological plasticity and nitrogen uptake of 59 plant species from the Great Plains grasslands, U.S.A. Basic Appl. Ecol. 2, 127–143.

Kondo, M., Aguilar, A., Abe, J., Morita, S., 2000. Anatomy of nodal roots in tropical upland and lowland rice varieties. Plant Prod. Sci. 3, 437–445.

Kozlowski, J., Konarzewski, M., 2004. Is West, Brown and Enquist's model of allometric scaling mathematically correct and biologically correct. Funct. Ecol. 18, 283–289.

Kurz, H., Sandau, K., 1998. Allometric scaling in biology. Science 281, 751–753.

Landsberg, J.J., Fowkes, N.D., 1978. Water movement through plant roots. Ann. Botany 42, 493–508.

Levang-Brilz, N., Biondini, M.E., 2002. Growth rate, root development and nutrient uptake of 55 plant species from the Great Plains grasslands, U.S.A. Plant Ecol. 165, 117–144.

Li, Y.Y., Shao, M.G., 2003. Responses of radial and axial hydraulic resistances in maize root to nitrogen availability. J. Plant Nutrition 26, 821–834.

McCully, M.E., Mallett, J.E., 1993. The branch roots of Zea 3. Vascular connections and bridges for nutrient cycling. Ann. Botany 71, 327–341.

Miller, D.M., 1981. Studies of root function in *Zea mays*. II. Dimensions for the root system. Canad. J. Botany 59, 811–818.

Nicotra, A.B., Babicka, N., Westoby, M., 2001. Seedling root anatomy and morphology: an examination of ecological differentiation with rainfall using phylogenetically independent contrasts. Oecologia 130, 136–145.

Peterson, C.A., 1988. Exodermal Casparian bands: their significance for ion uptake by roots. Physiologia Planta 72, 204–208.

Riley, K.F., Hobson, M.P., Bence, S.J., 2002. Mathematical Methods for Physics and Engineering, second ed. Cambridge University Press, UK.

Roose, T., 2000. Mathematical model of plant nutrient uptake. Ph.D. Dissertation. University of Oxford. Oxford, UK, 249p.

Roose, T., Fowler, A.C., 2004. A model for water uptake by plant roots. J. Theor. Biol. 228, 155–171.

Shane, M.W., McCully, M.E., Canny, M.J., 2000. Architecture of branch-root junctions in maize: structure of the connecting xylem and the porosity of pit membranes. Ann. Botany 85, 613–624.

Sharp, J.J., 1988. BASIC Fluid Mechanics. Butterworths & Company, Ltd., Boston.

Sherman, T., 1981. On connecting large vessels to small: the meaning of Murray's law. J. General Physiol. 78, 431–453.

Sperry, J.S., Stiller, V., Hacke, U.G., 2003. Xylem hydraulics and the soil-plant-atmosphere continuum: opportunities and unresolved issues. Agronomy J. 95, 1362–1370.

Steudle, E., 2000a. Water uptake by plant roots: an integration of views. Plant and Soil 226, 45–56.

Steudle, E., 2000b. Water uptake by roots: effects of water deficit. J. Exp. Botany 51, 1531–1542.

Steudle, E., 2001. The cohesion-tension mechanism and the acquisition of water by plant roots. Ann. Rev. Plant Physiol. Mol. Biol. 52, 847–875.

Steudle, E., Peterson, C.A., 1998. How does water get through roots? J. Exp. Botany 49, 775–788.

Taub, D.R., Goldberg, D., 1996. Root system topology of plants from habitats differing in soil resource availability. Funct. Ecol. 10, 258–264.

Varney, G.T., Canny, M.J., Wang, X.L., McCully, M.E., 1991. The branch roots of Zea. I. First order branches, their number, size and division into classes. Ann. Botany 67, 357–364.

Vercambre, G., Doussan, C., Pages, L., Habib, R., Pierret, A., 2002. Influence of xylem development on axial hydraulic conductance within Prunus root systems. Trees 16, 479–487.

West, G.B., Brown, J.H., Enquist, B.J., 1997. A general model for the origin of allometric scaling laws in biology. Science 276, 122–126.

West, G.B., Brown, J.H., Enquist, B.J., 1999. A general model for the structure and allometry of plant vascular systems. Nature 400, 664–667.

Zwieniecki, M.A., Thompson, M.V., Holbrook, N.M., 2003. Understanding the hydraulics of porous pipes: tradeoffs between water uptake and root length utilization. J. Plant Growth Regulation 21, 315–323.